Icarus 197 (2008) 556–571

Contents lists available at ScienceDirect

Icarus

www.elsevier.com/locate/icarus

Diagnostics of Titan's stratospheric dynamics using Cassini/CIRS data and the 2-dimensional IPSL circulation model

A. Crespin [a,*], S. Lebonnois [a], S. Vinatier [b], B. Bézard [b], A. Coustenis [b], N.A. Teanby [c], R.K. Achterberg [d], P. Rannou [e], F. Hourdin [a]

[a] *Laboratoire de Météorologie Dynamique, IPSL, CNRS/UPMC, Box 99, F-75252 Paris Cedex 05, France*
[b] *LESIA, Observatoire de Paris–Meudon, 5 place Jules Janssen, 92195 Meudon Cedex, France*
[c] *Clarendon Laboratory, AOPP, Department of Physics, University of Oxford, Parks Road, Oxford OX1 3PU, UK*
[d] *Department of Astronomy, University of Maryland, College Park, MD 20742, USA*
[e] *Service d'Aéronomie, IPSL, CNRS/UPMC/UVSQ, BP3, F-91371 Verrières-le-Buisson Cedex, France*

ARTICLE INFO

Article history:
Received 13 September 2007
Revised 30 April 2008
Available online 3 June 2008

Keywords:
Titan
Atmospheres, dynamics
Satellites, composition

ABSTRACT

The dynamics of Titan's stratosphere is discussed in this study, based on a comparison between observations by the CIRS instrument on board the Cassini spacecraft, and results of the 2-dimensional circulation model developed at the Institute Pierre-Simon Laplace, available at http://www.lmd.jussieu.fr/titanDbase [Rannou, P., Lebonnois, S., Hourdin, F., Luz, D., 2005. Adv. Space Res. 36, 2194–2198]. The comparison aims at both evaluating the model's capabilities and interpreting the observations concerning: (1) dynamical and thermal structure using temperature retrievals from Cassini/CIRS and the vertical profile of zonal wind at the Huygens landing site obtained by Huygens/DWE; and (2) vertical and latitudinal profiles of stratospheric gases deduced from Cassini/CIRS data. The modeled thermal structure is similar to that inferred from observations (Cassini/CIRS and Earth-based observations). However, the upper stratosphere (above 0.05 mbar) is systematically too hot in the 2D-CM, and therefore the stratopause region is not well represented. This bias may be related to the haze structure and to misrepresented radiative effects in this region, such as the cooling effect of hydrogen cyanide (HCN). The 2D-CM produces a strong atmospheric superrotation, with zonal winds reaching 200 $m\,s^{-1}$ at high winter latitudes between 200 and 300 km altitude (0.1–1 mbar). The modeled zonal winds are in good agreement with retrieved wind fields from occultation observations, Cassini/CIRS and Huygens/DWE. Changes to the thermal structure are coupled to changes in the meridional circulation and polar vortex extension, and therefore affect chemical distributions, especially in winter polar regions. When a higher altitude haze production source is used, the resulting modeled meridional circulation is weaker and the vertical and horizontal mixing due to the polar vortex is less extended in latitude. There is an overall good agreement between modeled chemical distributions and observations in equatorial regions. The difference in observed vertical gradients of C_2H_2 and HCN may be an indicator of the relative strength of circulation and chemical loss of HCN. The negative vertical gradient of ethylene in the low stratosphere at 15° S, cannot be modeled with simple 1-dimensional models, where a strong photochemical sink in the middle stratosphere would be necessary. It is explained here by dynamical advection from the winter pole towards the equator in the low stratosphere and by the fact that ethylene does not condense. Near the winter pole (80° N), some compounds (C_4H_2, C_3H_4) exhibit an (interior) minimum in the observed abundance vertical profiles, whereas 2D-CM profiles are well mixed all along the atmospheric column. This minimum can be a diagnostic of the strength of the meridional circulation, and of the spatial extension of the winter polar vortex where strong descending motions are present. In the summer hemisphere, observed stratospheric abundances are uniform in latitude, whereas the model maintains a residual enrichment over the summer pole from the spring cell due to a secondary meridional overturning between 1 and 50 mbar, at latitudes south of 40–50° S. The strength, as well as spatial and temporal extensions of this structure are a difficulty, that may be linked to possible misrepresentation of horizontally mixing processes, due to the restricted 2-dimensional nature of the model. This restriction should also be kept in mind as a possible source of other discrepancies.

* Corresponding author.
E-mail address: audrey.crespin@lmd.jussieu.fr (A. Crespin).

0019-1035/$ – see front matter
doi:10.1016/j.icarus.2008.05.010

1. Introduction

Because of its size, density and relatively low atmospheric temperature (surface temperature of 94 K), Titan has kept a dense atmosphere of nitrogen and methane (around 1.4% in the stratosphere; Niemann et al., 2005; Flasar et al., 2005), extending from the surface to roughly 1400 km in exobase altitude (Waite et al., 2005)—in contrast with the 400–500 km thickness of the Earth's atmosphere. Observations have revealed the presence of numerous hydrocarbons and nitriles in Titan's atmosphere. These compounds are produced in the upper atmosphere from the dissociation of methane and nitrogen by solar UV radiation, Saturn magnetospheric electrons, and cosmic rays, followed by an active photochemistry. The compounds are then transported downward to the lower atmosphere by dynamical processes, where most of them condense. Polymerization also occurs in the atmosphere, producing a thick haze layer, which covers the whole planet, masking its surface in the visible, except in small spectral windows in the infrared. The origin of this polymerization is still unknown and is the object of numerous experimental (e.g. Coll et al., 1999) and theoretical (Lebonnois et al., 2002; Wilson and Atreya, 2003) works; the difficulty is in understanding the production pathways leading to the formation of macromolecules, precursors of haze material.

In 1980, the Voyager 1 mission brought the first detailed observations of Titan's complex atmospheric system. Data remained limited until the Cassini–Huygens mission, which arrived at Saturn in July 2004. Both Huygens and Cassini have obtained the first in situ data from Titan and information about Titan's surface, atmospheric composition, aerosols, dynamics and clouds and their variability. Observations such as the presence of liquid hydrocarbons on the surface (Marouf et al., 2006)—signs of possible methane rainfall (Tomasko et al., 2005; Tokano et al., 2006) and likely the presence of lakes (Stofan et al., 2006)—suggest a methane cycle with similarities to the water cycle on Earth. Although the photochemical lifetime of methane in Titan's atmosphere is only around ten million years, it has been hypothesized that its replenishment into the atmosphere could be due to cryovolcanism induced by Saturn's gravitational tides, and may have been limited to three episodes during Titan's history (Tobie et al., 2006; Sotin et al., 2005). But, the exact methane source is not yet known. Cassini has also revealed variations in the altitude of the detached haze layer, observing it at around 500 km during northern winter (Porco et al., 2005), while Voyager 1 had observed it much lower, at around 350 km altitude after the northern spring equinox. Whether this variation is related to season or to variations of other parameters (e.g. the solar cycle or Saturn's magnetosphere) is still an open question.

Before the Cassini–Huygens mission, information about temperature and abundance of molecules in Titan's stratosphere was limited. Analysis of data from the infrared spectrometer Voyager 1/IRIS taken during a single flyby of Titan in 1980, allowed scientists to retrieve abundances of C_2H_2, C_2H_4, C_2H_6, CH_3C_2H, C_3H_8, C_4H_2, C_2N_2, HCN and HC_3N between 53° S and 70° N (Coustenis et al., 1991; Coustenis and Bézard, 1995). Enrichment of some of these molecules was observed at high northern latitudes. Today, the contribution of the Cassini mission to the knowledge of Titan's atmosphere is considerable. In particular, the Composite Infrared Spectrometer (CIRS), which records spectra between 10 and 1500 cm^{-1}, is dedicated to the study of stratospheric temperatures and molecular abundances below 500 km. This spectral range displays emission features of numerous hydrocarbons (such as CH_4, C_2H_2, C_2H_4, C_2H_6, C_3H_8, CH_3C_2H, C_4H_2, C_6H_6) and nitriles (HCN, HC_3N, C_2N_2), as well as oxygen compounds (CO_2, CO, H_2O). CIRS data has been used to retrieve temperature and gas abundance maps, as well as vertical temperature and mixing ratio profiles with a vertical resolution of about 30 km (comparable to the pressure scale height in Titan's stratosphere). A crucial point is that CIRS acquires spectra during most Titan flybys (roughly one each month) and gives reasonable coverage at most latitudes. Therefore, throughout the Cassini mission (now extended until 2010), a systematic study of the stratosphere can be undertaken and CIRS should allow the characterisation of seasonal variations in Titan's stratosphere. Cassini/CIRS provide important information on vertical and latitudinal contrasts and enrichments of chemical species in the winter polar region, and together with theory/modeling provide additional information on the dynamics of the atmosphere at different seasons. Together with recent ground-based observations, they also provide information on the seasonal evolution of the stratospheric composition.

After the development of the first models of Titan's atmosphere, the importance of including couplings between the dynamics, photochemistry and microphysics has emerged. Analysis concerning dynamics (Hourdin et al., 1995), chemical composition (Bézard et al., 1995; Coustenis and Bézard, 1995), haze (Rannou et al., 1995, 1997), and thermal structure (Flasar et al., 1981; Coustenis and Bézard, 1995) have indicated the existence of a strong interaction between these processes. Using a 2-dimensional version of the general circulation model developed by Hourdin et al. (1995), further studies have been conducted to include microphysical and photochemical models coupled to radiative transfer and dynamics, and important interactions were studied between 1996 and 2004 (Lebonnois et al., 2001; Rannou et al., 2002, 2004; Hourdin et al., 2004). The most recent development of this coupled model has been the implementation of a cloud scheme (Rannou et al., 2006), yielding significant progress in understanding the tropospheric methane cycle (also studied in Tokano et al., 2001; Mitchell et al., 2006). This model has helped in interpreting much of the Voyager 1 data, taken just after spring equinox conditions on Titan, in particular for latitudinal distributions of trace compounds. The observed enrichment of most chemical species in the winter polar region was attributed to downward advection of chemical species in the descending branch of the meridional circulation (Lebonnois et al., 2001). Latitudinal thermal contrasts and zonal winds are also in good agreement with available pre-Cassini observations (Rannou et al., 2004; Hourdin et al., 2004), showing the strong interdependence of dynamics, haze, and radiative transfer processes.

The goal of this paper is to interpret new Cassini and ground-based observations with the support of the IPSL atmospheric circulation model (2D-CM), using in particular the chemical compound distributions as tracers of dynamical processes. Minor species such as C_2H_2, C_2H_4, C_2H_6, C_3H_8 and HCN have lifetimes greater than roughly 10^6 s, at 300 km (Wilson and Atreya, 2004), which is longer than typical dynamical time scales in Titan's stratosphere (roughly 7.0×10^5 s, at 300 km; Hourdin et al., 2004). One must keep in mind that the 2D-CM involves all components of the coupled model, including the aerosol structure, which strongly influences dynamics (Rannou et al., 2004). We focus on the comparison with recent Cassini/CIRS observations of temperature and composition. For dynamical validation studies we also use observations from the Huygens probe experiments (e.g. vertical zonal wind profile at 10° S). Other Earth-based measurements are used to complement this study, including Keck Observatory Long Wavelength Spectrometer data (Roe et al., 2004); Institute of Millimetric Radio Astronomy (IRAM) and Pico Veleta millimeter observations (Tanguy et al., 1990; Hidayat et al., 1997; Marten et al., 2002); and sub-millimeter array observations (Gurwell, 2004). We also use data from Earth-bound measurements, such as the Infrared Space Observatory data reported by Coustenis et al. (2003). These observations complement the space missions, especially in terms of temporal coverage over one Titan's year. At present, the available observational dataset covers almost one complete Titan year, from

the Voyager 1 flyby in 1980 (northern spring equinox, $Ls \sim 9°$) to Cassini (northern winter, $Ls \sim 300°$). With such a complete 2D-CM, the purpose of this paper is to understand how the processes included in the model can explain some of the observed features. The model reproduces several characteristics of aerosols' distributions and thermal structure. We use the model to test how chemical distributions behave under such dynamical forcings.

We first present the two-dimensional (latitude–altitude) circulation model of Titan's atmosphere, which extends up to approximately 500 km, in the lower mesosphere, and its most recent updates (Section 2). Then the CIRS observations used to validate the model are described in Section 3. Section 4 is dedicated to temperature structure and zonal winds. Results related to the stratospheric composition are detailed in Section 5, with emphasis on the circulation characteristics that may be deduced from the observed distributions.

2. The IPSL 2-dimensional circulation model

The Laboratoire de Météorologie Dynamique and the Service d'Aéronomie have been collaborating for many years within Institute Pierre-Simon Laplace to develop a general circulation model of Titan's atmosphere. This model is currently 2-dimensional, extending from the surface up to roughly 500 km altitude (50 levels), and from pole to pole (3.75° resolution).

The earliest simulations of the Titan's atmospheric dynamics (Hourdin et al., 1995) were performed at LMD with a full 3-dimensional model, based on the dynamical core of the LMD general circulation model used for climate studies on both Earth (see e.g. Hourdin et al., 2006) and Mars (Forget et al., 1999). In these early simulations, in which composition did not vary with latitude, a strong superrotation was obtained by the Gierash–Rossow mechanism: upward zonal momentum transport by the mean meridional circulation, and equatorward zonal momentum transport by planetary waves, which were shown to be related to barotropic instability of mid-latitude jets.

However, when developing the coupling between atmospheric dynamics, chemistry and haze microphysics, the choice was made to instead use a 2-dimensional model, obtained by removing the longitudinal variations from the 3-dimensional core. In this 2-dimensional model, the non axisymmetric component of the flow is not represented explicitely. Because (nonaxisymmetric) planetary waves play a major role in building and maintaining the superrotation, and because they also transport trace species in latitude, a specific study was devoted to the characterization of the transport by those waves (Luz and Hourdin, 2003), which led to a parameterization of the wave transport for the 2-dimensional model (Luz et al., 2003). This parameterization acts as a diffusion in latitude of both vorticity and trace species, with the intensity of the diffusion related to the intensity of barotropic instability of the mean zonal flow. For the vorticity (and angular momentum), when the criterium for barotropic instability is met in the 2D-CM, latitudinal dissipation is applied with a time constant directly related to the diagnosed degree of instability. The relation between these two variables has been initially evaluated using a one-layer 2-dimensional longitude–latitude model of the shallow water equations in a quasi-steady state regime with fully developed planetary waves forced by barotropic instability details are in (Luz et al., 2003). The parametrization was also validated a posteriori by comparing the effect of the parametrization in the 2D-CM with the effect of the fully developed planetary waves in the 3D simulations. For trace species, the diffusion coefficient is parameterized similarly (Luz et al., 2003), while the explicit transport of trace species by the axisymmetric flow is computed based on finite volume advection schemes introduced in the GCM by Hourdin and Armengaud (1999).

In the uppermost layers of the 2D-CM, a sponge layer is included, with Rayleigh friction dumping horizontal winds to zero. For vertical dissipation, the 2D-CM includes a boundary-layer scheme that induces some vertical turbulent mixing close to the surface (see Hourdin et al., 1995). No other vertical turbulent diffusion is taken into account.

A microphysical model describing the photochemical haze is also included (Cabane et al., 1992; Rannou et al., 1995). Coupling between the haze layer, radiation field and dynamics is taken into account. The source function of the aerosols is fixed, located at roughly 400 km altitude at all latitudes. The modeled haze distribution is able to reproduce many observations, such as Titan's albedo, its seasonal North–South asymmetry, and the structure of the main and detached haze layers (Rannou et al., 2002, 2004).

The 2D-CM we use here is the same as in Rannou et al. (2004), with active photochemistry included. The photochemistry module is based on the initial photochemical model by Toublanc et al. (1995), adapted for the 2D-CM, and updated to take into account new photochemical data (Wilson and Atreya, 2004; Vuitton et al., 2006; Hébrard et al., 2006), benzene photochemistry (Lebonnois, 2005), and heterogeneous recombination of atomic hydrogen on the aerosols (Lebonnois et al., 2003a; Sekine et al., 2008). A parameterization for photochemical production of aerosols developed by Lebonnois et al. (2002) has also been included and acts. This parametrization is taken into account as a sink for atmospheric compounds. However, the obtained aerosol production rate it yields does not peak at the right altitudes to reproduce the distributions observed on Titan. Therefore, this coupling is not activated in the simulations presented here. The photochemical model currently includes 44 species with 343 reactions, and is computed once per Titan day, with diurnal means used for photodissociation rates (no diurnal variations of the composition have yet been observed, and they are considered for the moment as negligible).

At the upper boundary, the exchange flux between the upper atmosphere and the upper layer of the model is taken into account for all chemical species. These exchange fluxes are computed using an updated version of the two-dimensional model of Titan's atmosphere used by Lebonnois et al. (2001), which computes the atmospheric composition up to 1200 km altitude. The photochemistry in this model is the same as the one used in our 2D-CM photochemistry module. The fluxes obtained around 500 km altitude depend upon both season and latitude. For most compounds, the flux is maximum over the summer pole, minimum (several orders of magnitude lower) over the winter pole, and almost constant with time over the equator. The upper boundary fluxes have a strong influence on the mean stratospheric abundance of most compounds. Unfortunately, the photochemical model used to compute them is not completely satisfying in the upper atmosphere, especially when compared to new observations by Cassini/INMS. Modeled composition is consistent with observations by Cassini/UVIS (Shemansky et al., 2005), and the reanalysis of Voyager 1/UVS data (Vervack et al., 2004). However, the photochemical model still suffers from approximations made for the photochemistry of the upper atmosphere above 500 km, where most of these species are produced. For example, ion-neutral chemistry is not taken into account, though it may be important for high altitude chemistry (Wilson and Atreya, 2004). Therefore, it is not surprising that in order to fit observed stratospheric abundances, these fluxes have to be adjusted for some molecules. These adjustments have been made for C_2H_2, C_2H_6, C_3H_8 and HCN. Some of these upper boundary fluxes used in the model are tabulated in Table 1.

At the lower boundary, the methane mole fraction is fixed at the surface (5%). It follows saturation up to the tropopause, yielding a mole fraction of 1.5% at higher levels. These values approximate the Huygens/GCMS measurements (Niemann et al., 2005). For all other compounds, surface fluxes (exchanges between sur-

Table 1
Some of the upper boundary fluxes (top of the model) used as upper boundary condition (units of molecules $cm^{-2}\,s^{-1}$, referred to 500 km altitude, positive values are downward)

Molecule	Summer pole	Equator	Winter pole
C_2H_2[a]	2.0×10^{10}	1.5×10^{10}	2.6×10^{7}
C_2H_4	3.2×10^{8}	4.5×10^{8}	-2.5×10^{6}
C_2H_6[a]	5.0×10^{10}	4.3×10^{10}	2.9×10^{8}
CH_3C_2H	4.8×10^{7}	4.1×10^{7}	-3.7×10^{5}
C_3H_8[a]	1.1×10^{9}	6.9×10^{8}	-3.9×10^{6}
C_4H_2	7.9×10^{6}	4.9×10^{6}	3.3×10^{3}
C_6H_6	3.9×10^{7}	2.7×10^{7}	1.0×10^{4}
HCN[a]	1.4×10^{9}	1.4×10^{9}	6.6×10^{7}
CH_3CN	1.8×10^{8}	1.1×10^{8}	5.1×10^{5}
HC_3N	4.7×10^{7}	2.4×10^{7}	1.9×10^{4}

[a] Values tuned to fit stratospheric observations.

face and the first atmospheric layer) are fixed to zero as described in the photochemical scheme by Toublanc et al. (1995).

The reference simulation discussed in this paper has been run for ten Titan years, yielding a stabilized seasonal cycle for all variables. This reference simulation is made available through a public database, accessible on the web at http://www.lmd.jussieu.fr/titanDbase (Rannou et al., 2005).

3. CIRS observations

Most of the temperature and abundance observations that we use here are deduced from the Cassini/CIRS instrument.

Two types of observations are recorded by CIRS. Some data are acquired in a nadir viewing geometry, where the line-of-sight intercepts Titan's surface, and other observations are recorded at the limb, where the line-of-sight is horizontal and intercepts only the atmosphere.

The CIRS nadir spectra characterize various regions on Titan from the North pole to the South pole with a variety of emission angles. For comparison with the 2D-CM, we use here the results obtained by Teanby et al. (2006, 2008) and Coustenis et al. (2007a, 2007b). These authors have used 0.5 and 2.5 cm^{-1} spectral resolutions, recorded between the Tb and T20 flybys of Titan to retrieve the abundances of CH_4, CH_3D, C_2H_2, C_2H_4, C_2H_6, CH_3C_2H, C_3H_8, C_4H_2, C_6H_6, HCN, HC_3N, C_2N_2 and CO_2 between 80° S and 80° N. Using these data, temperature and composition can be retrieved, with sensitivity generally focused at pressures between 0.1 to 10 mbar. Vertical composition profiles cannot be retrieved from the nadir observations, but vertical profiles derived from limb data analysis are tested and scaled to give the best fit. Therefore the nadir data generally yield meridional variations and maps of the chemical and thermal structure focused in a given part of the middle stratosphere.

The upper stratosphere, stratopause and lower mesosphere, can be sounded using limb viewing observations. These observations generally probe levels between 1 μbar (500 km) and 5 mbar (~120 km) and allow retrieval of both temperature and abundance vertical profiles. The inversion method for vertical temperature and composition profiles is described in Teanby et al. (2007) and Vinatier et al. (2007). For comparisons with the 2D-CM, we use here temperature profiles retrieved at 58° S, 67° N, 82° N (Teanby et al., 2007, high spectral resolution dataset: 0.5 cm^{-1}), 15° S (Teanby et al., 2007; Vinatier et al., 2007), and 80° N (Vinatier et al., 2007), as well as the latitudinal temperature profiles derived from the meridional temperature cross-section published in Flasar et al. (2005). Meridional temperature cross-sections (latitude–altitude) (80° S–80° N) retrieved by Teanby et al. (2007) using a low spectral resolution dataset (13.5 cm^{-1}) are also considered for comparison, as well as the in situ temperature profile deduced from Huygens/HASI data at 10° S (Fulchignoni et al., 2005).

As described in Teanby et al. (2007) and Vinatier et al. (2007), the retrieved temperature profiles have been used to model the observed emission bands of molecules in order to deduce their vertical mixing ratio profiles. Through an inversion algorithm, the vertical abundance profiles of HCN, HC_3N and C_2H_2 were derived at 58° S, 67° N, 82° N (Teanby et al., 2007), and 15° S (Teanby et al., 2007; Vinatier et al., 2007). We also consider in this study the mixing ratio vertical profiles of the hydrocarbons C_2H_4, C_2H_6, C_3H_8, C_4H_2, and CH_3C_2H retrieved at 15° S and 80° N by Vinatier et al. (2007).

4. Dynamical and thermal structure

4.1. Atmospheric temperatures

Observations of the temperature structure at different seasons and latitudes are summarized in Table 2. The modeled thermal structure strongly depends on the structure of the haze layers in the model. In order to reproduce haze structure observed at the Voyager 1 epoch, the altitude of the haze production was fixed at the 0.01 mbar pressure level (roughly 400 km altitude). In these conditions, the haze structure and the stratospheric thermal structure observed by Voyager 1 are well reproduced (Rannou et al., 2002, 2004). Cassini observations have shown a detached haze layer at approximately 500 km altitude (Porco et al., 2005), much higher than was observed during the Voyager 1 flyby (around 300–350 km altitude). The origin of this change is not understood and cannot be reproduced by the model, since the position of the detached haze layer currently occurs close to the top of our model domain. The impact of a test simulation with an elevated aerosol production source on the modeled thermal structure, and therefore on dynamics, is described in Section 4.3. The discrepancy between observed and modeled haze distributions has significant consequences on the temperature distributions, as shown in Fig. 1.

The modeled thermal structure presents similarities with Cassini/CIRS observations (Teanby et al., 2007; Achterberg et al., 2008). From the summer (i.e. southern) polar region to roughly 30° N, only small latitudinal variations are found in the temperature field. On the other hand, in the winter (i.e. northern) polar region, temperatures increase (respectively, decrease) towards the pole in the upper (respectively, lower) stratosphere. The temperature increase at the stratopause (at around 0.01 mbar) is due to adiabatic heating in the descending branch of the meridional circulation, while the temperature minimum at lower altitudes is mainly related to the increased radiative cooling due to high infrared haze opacity in the region of polar night, not balanced by direct absorption of solar visible radiation. At the Voyager 1 epoch, latitudinal temperature profiles observed at 0.4 and 1 mbar were well reproduced by 2D-CM simulations (see Fig. 14 of Rannou et al., 2004). But for the Cassini epoch, due to the discrepancy in the altitude of the haze layers, the resulting modeled dynamical and thermal structures seem to be located at lower altitudes than the corresponding observed structures. As a consequence, the modeled latitudinal profile at a given pressure level (1.8 mbar) is not in agreement with observations, but a similar profile is found in the 2D-CM slightly lower in the stratosphere, as shown in Fig. 2 for 4 mbar. From these comparisons, the vertical profile of haze extinction clearly has an impact on the vertical extent of the circulation and further on the thermal structure.

Fig. 3 compares vertical temperature profiles from the 2D-CM to available observations. The model systematically overestimates temperatures at pressures less than about 0.05 mbar, and therefore does not correctly reproduce the observed stratopause. This

Table 2
Available observations of Titan's temperature structure and zonal winds at different seasons and latitudes

Observations	Reference	Season (*Ls*, degrees)	Latitude (degrees)	Altitude range (km)	Pressure range (mbar)
Temperature structure					
Voyager1/RSS (vertical profile)	Lindal et al. (1983)	9	6° N ingress and 8° S egress	0–200	
Voyager1/IRIS	Flasar and Conrath (1990)	9	(high S–high N)	180; 230	1; 0.4
(latitudinal profiles)	Coustenis and Bézard (1995)	9	53° S–70° N	180; 230	1; 0.4
Ground-based	Tanguy et al. (1990)	130	Disk average	0–550	$1400–6.7 \times 10^{-4}$
(vertical profiles)	Hidayat et al. (1997)	180	Disk average	0–600	$1400–2.6 \times 10^{-4}$
Huygens/HASI (vertical profile)	Fulchignoni et al. (2005)	300	10° S	0–1400	$1400–10^{-8}$
Cassini/CIRS	Flasar et al. (2005)	300	80° S–60° N	100–250	10–0.2
(meridional maps)	Teanby et al. (2007)	300	80° S–85° N	140–500	3–0.002
	Achterberg et al. (2008)	300	90° S–85° N	120–450	5–0.005
(vertical profiles)	Coustenis et al. (2007b)	300	50° N–70° N nadir	~180–350	1–0.03
	Coustenis et al. (2007b)	300	60° S–35° N nadir	~120–320	5–0.06
	Vinatier et al. (2007)	300	15° S nadir and limb, 80° N limb	195–490, 170–495	0.8–0.002, 0.9–0.002
	Teanby et al. (2007)	300	15° S, 82° N	140–500	3–0.002
Zonal wind structure					
Cassini/CIRS	Flasar et al. (2005)	300	80° S–60° N	100–250	10–0.2
(meridional maps)	Achterberg et al. (2008)	300	90° S–85° N	120–450	5–0.005
(vertical profile)	Bird et al. (2005)	300	10° S	0–140	1400–3

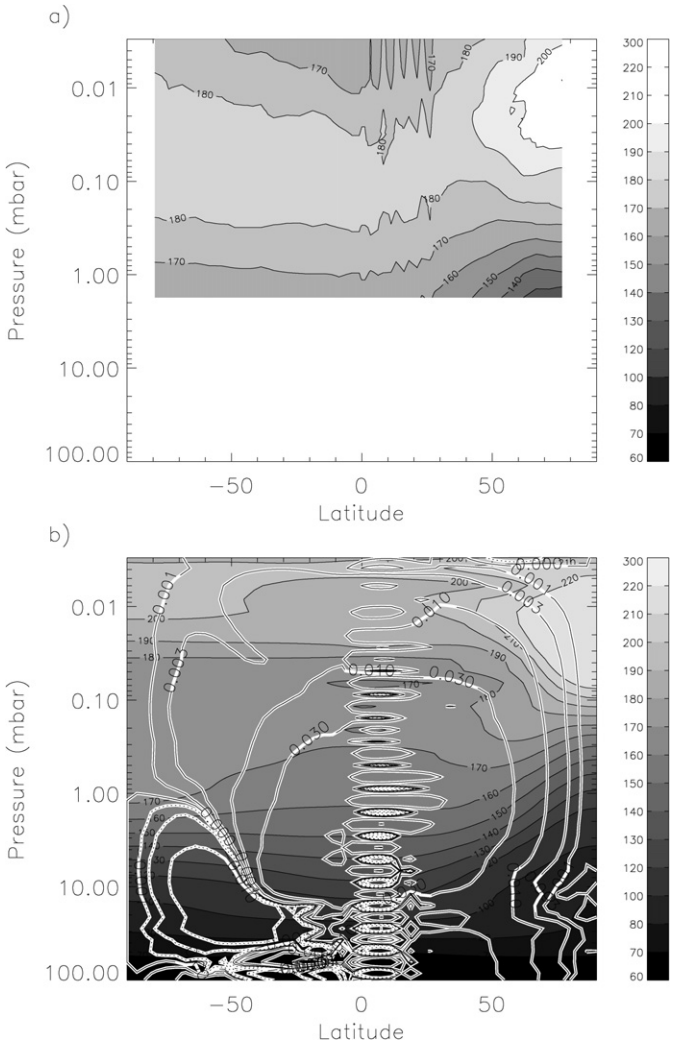

Fig. 1. (a) Temperature meridional map (latitude–altitude) from Teanby et al. (2007) (K); (b) corresponding temperature meridional map modeled with the 2D-CM (K). Contours of the stream function are also plotted (units of 10^9 kg s^{-1}, solid line is clockwise rotation, dashed line is anti-clockwise). Note that the troposphere is not shown.

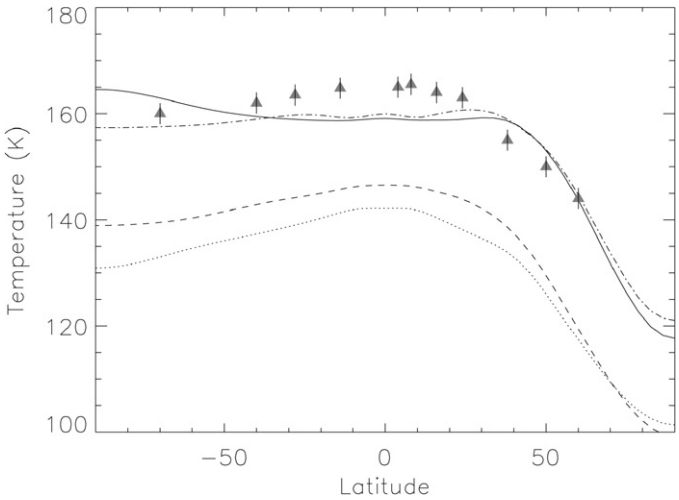

Fig. 2. Latitudinal profile of T observed by Cassini/CIRS at 1.8 mbar gray triangles, from Flasar et al. (2005), compared to 2D-CM (solid line: 1.8 mbar; dashed line: 4 mbar). The profiles obtained with the test simulation discussed in Section 4.3 are also plotted (dash-dotted line: 1.8 mbar; dotted line: 4 mbar).

is probably due to the warming induced by shortwave absorption of the detached haze, which is actually observed higher than predicted by the model. The same signature should be present at about 500 km in the data. This bias may also be related to other aspects of the model. Several other significant effects are not taken into account including the coupling between the modeled distributions of ethane (C_2H_6) and acetylene (C_2H_2) and the thermal structure, as well as the cooling effect of hydrogen cyanide (HCN). These effects were discussed by Lebonnois et al. (2003b), who showed that a small increase in these compounds' abundance in the upper region of the 2D-CM, as well as taking the radiative impact of HCN into account, has a cooling effect at pressures less than 0.1 mbar. Indeed, a test simulation done in parallel to the main simulation, but coupling the modeled distributions of C_2H_2, C_2H_6 and HCN (as in Lebonnois et al., 2003b) with the cooling rates computations, yielded temperatures 20 K cooler than in Fig. 1b at winter high latitudes, above 0.1 mbar, and a clear stratopause around 0.01 mbar at other latitudes.

At the tropopause, the temperature is slightly underestimated in the simulations. In this region, the control by the haze struc-

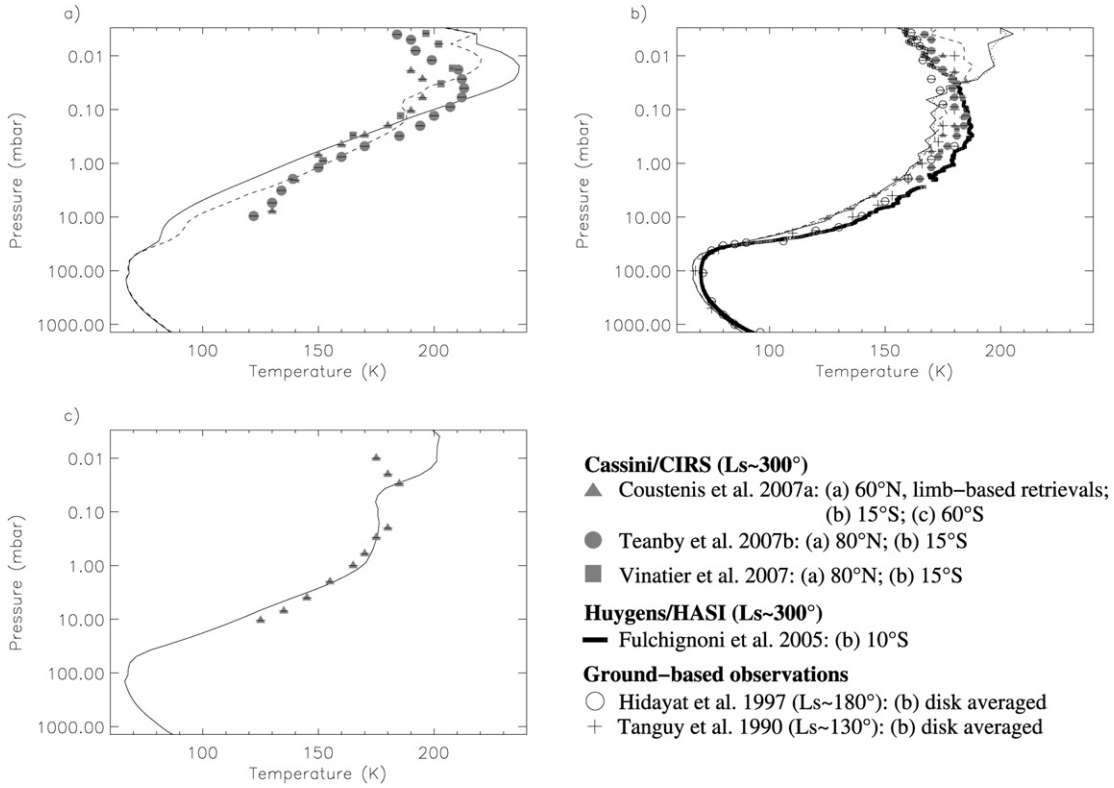

Fig. 3. Observed vertical T profiles (see legends for references), compared with the 2D-CM. (a) Northern mid- and high latitudes (winter): Cassini/CIRS (80° N, 60° N), with 2D-CM profiles at $Ls = 300°$, 80° N (solid line) and 60° N (dashed line); (b) tropics and disk-average: Huygens/HASI (10° S), Cassini/CIRS (15° S) and ground-based observations, with 2D-CM profiles at $Ls = 300°$, equator (solid line) and 15° S (dotted line), and $Ls = 180°$, equator (dashed line); (c) southern mid-latitudes (northern winter): Cassini/CIRS (60° S), with 2D-CM profiles at $Ls = 300°$, 60° S (solid line).

ture is strong since the haze opacity regulates the amount of solar flux reaching the ground. On the other hand, the infrared radiative transfer is controlled by pressure induced absorption which is also difficult to model exactly; we use the model of Courtin (1988) which would need an upgrading in order to take into account the collision-induced absorption due to CH_4–N_2 (Borysow and Tang, 1993; Samuelson et al., 1997). However, the impact of the fine thermal structure in the troposphere is minor on the stratosphere circulation and latitudinal thermal structure.

The thermal structure variations induced by subsidence in the winter polar region appears to be overestimated in the 2D-CM when compared to the observed effects in the mesosphere (Fig. 3a), although it must be noted that CIRS data do not yield information below the 10 mbar region at high winter latitudes (Teanby et al., 2008; Vinatier et al., 2007; Achterberg et al., 2008). This overestimate may be related to the fact that the 2D-CM simulations do not reproduce the Cassini/ISS observations in the main haze layer structure over the northern polar region. Indeed, a drop in the upper altitude of the main haze layer over this region, below a hood linked to the detached haze layer, is visible in some Cassini/ISS images (http://photojournal.jpl.nasa.gov/, images PIA09007 or PIA08214). It should also be noted that for condensation which occurs above 50 km, the corresponding release of latent heat and cloud opacity are not accounted for in this simulation. In the polar region, these two effects may explain a higher temperature in the observations than in the model in the lower stratosphere.

4.2. Zonal wind

The 2D-CM produces superrotation of the atmosphere, with strong zonal winds in the stratosphere, reaching almost 200 $m\,s^{-1}$ at high winter latitudes between 200 and 300 km altitude (0.1–1 mbar), and up to 130 $m\,s^{-1}$ in the equatorial region. This simulated superrotation is built up through the Gierasch–Rossow mechanism (Gierasch, 1975). The annual mean meridional circulation consists of two equator-to-pole thermal cells, analogous to the Brewer–Dobson stratospheric circulation on Earth. This circulation transports angular momentum in the upper stratosphere towards polar regions, whereas barotropic instabilities developing on the equatorward flank of the jet induce momentum redistribution towards the equator. In the 2D-CM, this transport is parameterized (Luz et al., 2003), as the model cannot generate explicitely these waves.

The modeled meridional circulation is strongly influenced by seasons. During a long season around the solstices, the meridional circulation is dominated by one cell which extends from summer to winter polar regions, where a strong zonal jet is produced. The ascending branch is located at summer latitudes. Around the equinoxes, the ascending branch moves from one hemisphere to the other, forming two cells (Hourdin et al., 1995, 2004; Rannou et al., 2004). The mean meridional circulation is qualitatively the same in the 2-dimensional simulations presented here and in that obtained initially with the 3-dimensional general circulation model of Hourdin et al. (1995). The main difference consists in a phase shift in seasons, due to the coupling between haze and dynamics (Rannou et al., 2004), not accounted for in the 3-dimensional version, which makes the winter circulation regime persists somewhat longer after spring equinox.

The same Gierasch–Rossow mechanism, with upward transport of angular momentum by the mean meridional circulation, thus explains the superrotation both in the 2-dimensional and 3-dimensional versions. The transport towards the equator by planetary waves is also qualitatively similar in the two versions. It is done by and occurs via explicitely resolved planetary waves in the 3-dimensional model while it is parameterized in the 2-

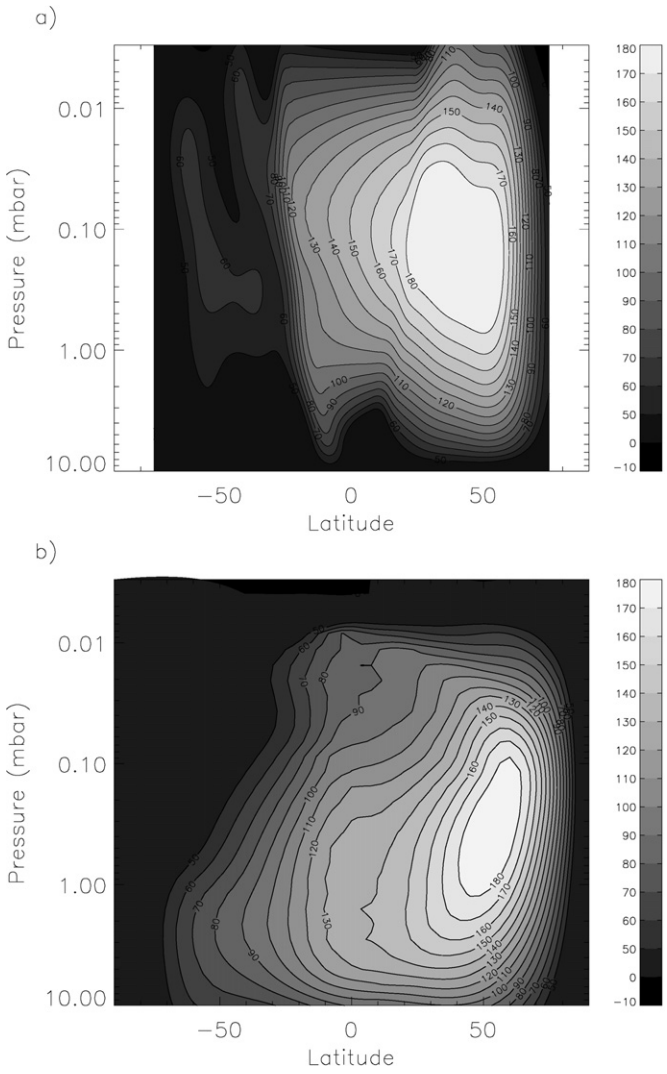

Fig. 4. Zonal wind meridional maps (latitude–altitude). (a) Cassini/CIRS data and the thermal wind equation (Achterberg et al., 2008), and (b) 2D-CM output for the Cassini epoch ($Ls = 300°$) (units of $m\,s^{-1}$).

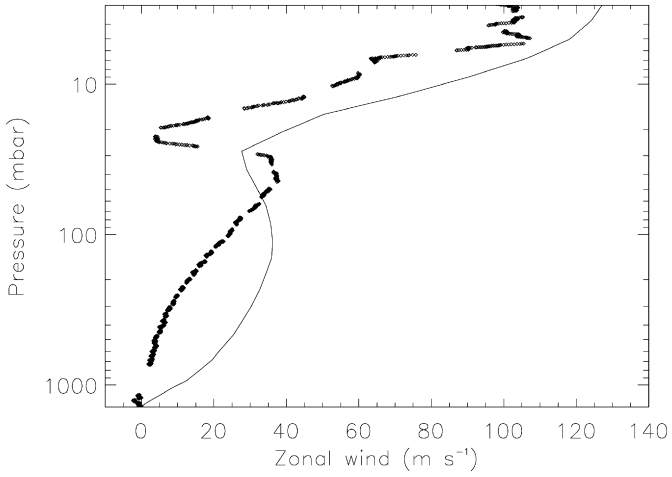

Fig. 5. Vertical profile of the zonal wind measured with the Huygens/DWE experiment at 10° S (bold line; Bird et al., 2005), compared with the corresponding 2D-CM zonal wind profile (solid line) ($m\,s^{-1}$).

dimensional version (as explained in Section 2). In 3-dimensional simulations, these waves take their energy from the barotropic instability of the mid-latitude stratospheric jets. It must however be kept in mind that the parameterization used in the 2-dimensional version is only an approximate representation of the effect of a particular subset of the planetary waves present in the real Titan's atmosphere.

The modeled zonal winds agree quite well with winds reconstructed from stellar occultation observations, corresponding to southern ($Ls \sim 128°$; Hubbard et al., 1993) and northern winter ($Ls = 290°$; Sicardy et al., 2006), as shown by Rannou et al. (2002). In Fig. 4, the modeled zonal wind field is shown at the Cassini epoch ($Ls \sim 300°$), together with the zonal wind field retrieved using temperatures obtained from CIRS spectra, based on the thermal wind equation (Flasar et al., 2005; Achterberg et al., 2008). The lower boundary value for the calculation of the thermal wind was imposed at 10 mbar (roughly 55 $m\,s^{-1}$) to correspond to Huygens/DWE measurements. For an atmosphere in cyclostrophic balance, the zonal wind and temperature fields are coupled through the thermal wind equation. Therefore, what we discussed for the latitudinal temperature gradient at 1.8 mbar at the winter mid-latitudes (Fig. 2) is consistent with the fact that the vertical gradient of the zonal wind between 10 mbar and the core of the winter jet is well rendered by the model. The location and the intensity of the jet are also relatively well reproduced. Improving remaining discrepancies between the modeled and observed dynamical structure (e.g. vertical gradient of the zonal wind in the lower stratosphere in equatorial regions) will probably require a realistic 3-dimensional model, explicitly representing all kinds of nonaxisymmetric motions.

Fig. 5 shows a comparison of the zonal wind vertical profile deduced from the Huygens/DWE experiment (Bird et al., 2005) with the corresponding 2D-CM profile. Although the modeled wind is stronger than observations at pressures less than ∼15 mbar, the strong vertical gradient in the stratosphere is well reproduced because the model has good representation of the latitudinal temperature gradient, which is linked to the vertical wind gradient via the thermal wind equation. A minimum in the zonal wind is seen in the 2D-CM at an altitude similar to the layer "with surprisingly slow wind" (Bird et al., 2005) detected by DWE during the Huygens descent, though it does not decrease to near zero as in the observations, but to ∼30 $m\,s^{-1}$, which may be due to the coarse vertical resolution of the 2D-CM. Radiative forcing in this region is very weak, and dynamic time scales are very long in the lower stratosphere and troposphere. In this transition layer, the equator is colder than the poles in the 2D-CM inducing a strong decrease in the zonal wind with height, according to cyclostrophic balance, whereas at other altitudes, the poles are generally colder than the equator. This is represented in the 2D-CM meridional cross-section (latitude–altitude) of equator-pole temperature contrasts (Fig. 6). An explanation for this inversion of the latitudinal temperature gradient would require further investigations which is beyond the scope of this paper. It may be related to the presence of a small cell in the lower stratosphere (60–1 mbar), between the summer pole and the ascending motion of the dominant pole-to-pole cell (see Fig. 1b). This ascending branch goes from 30–40° at 6 mbar to the summer pole at roughly 1 mbar. This secondary cell is therefore a remnant of the previous season's cell, and the implications of its presence in the simulations will be more extensively discussed in Section 5.3.

This secondary cell is forced by the latitudinal distribution of aerosols. Fig. 7 shows the net temperature tendencies due to both solar heating and infrared cooling at the Cassini epoch ($Ls \sim 300$). A net cooling is visible between approximately 10 and 1 mbar at southern latitudes. Except in this region, the summer stratosphere is globally warming, whereas the winter stratosphere is cooling, inducing the dominant pole-to-pole circulation. The presence of this cooling region over the summer pole explains the small secondary

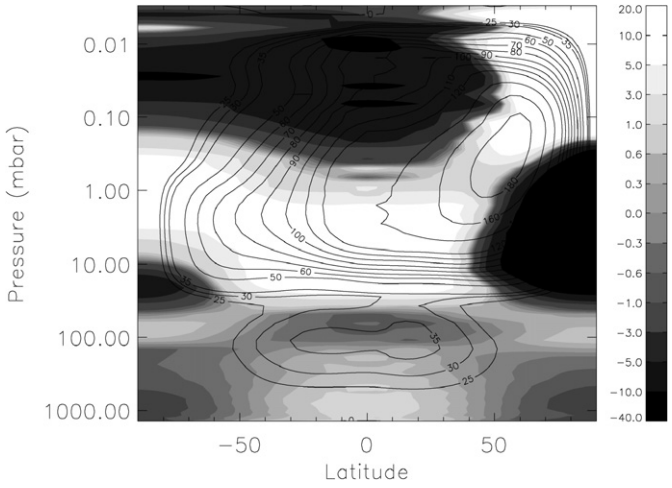

Fig. 6. Latitudinal contrasts in the 2D-CM temperature field (K) at Cassini epoch ($Ls \sim 300°$) showing difference between temperature and its latitudinal average. Contours are the corresponding zonal wind.

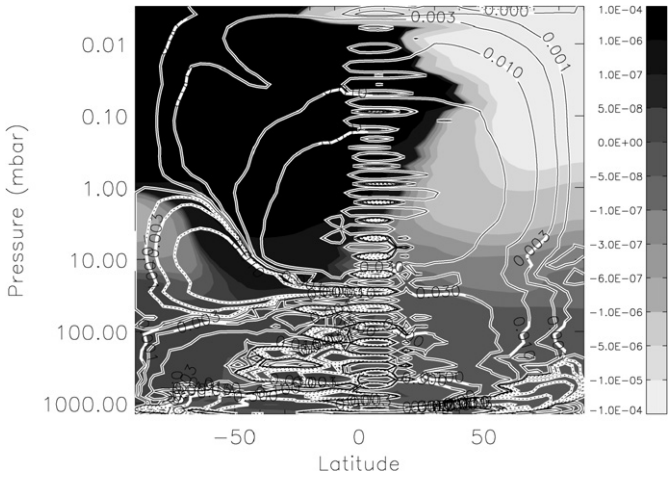

Fig. 7. Net radiative temperature tendencies during the Cassini epoch ($Ls \sim 300°$) ($K\,s^{-1}$). The stream function is also shown with contours (units of 10^9 $kg\,s^{-1}$, solid line is clockwise rotation, dashed line is anti-clockwise).

cell. In this region, the abundance of haze is still enriched compared to mid-latitudes. Therefore, both solar heating and infrared cooling are enhanced, but above the pole, the net effect is dominated by cooling.

At pressures greater than 100 mbar, the modeled zonal wind is too strong in the troposphere, compared to the DWE measurements. The discrepancy between observations and the 2D-CM in the troposphere suggests that decoupling is too strong between the ground and the tropospheric circulation, which may be due either to an underestimation of the vertical turbulent or convective mixing in the model, or to three-dimensional processes not captured in this 2D-CM. A specific study focused on lower stratospheric and tropospheric dynamics is needed to better understand what controls these discrepancies.

4.3. Influence of the altitude of the detached haze layer

In order to try to reconcile the modeled thermal structure with CIRS observations, we ran a sensitivity experiment with a source function for the aerosol fixed at 1 μbar, instead of 10 μbar in the reference simulation. This places the haze production altitude in the uppermost layer of the model. In this region, wind speeds are affected by the sponge layer, and the build up of haze may also be affected by the upper boundary. Therefore, this simulation

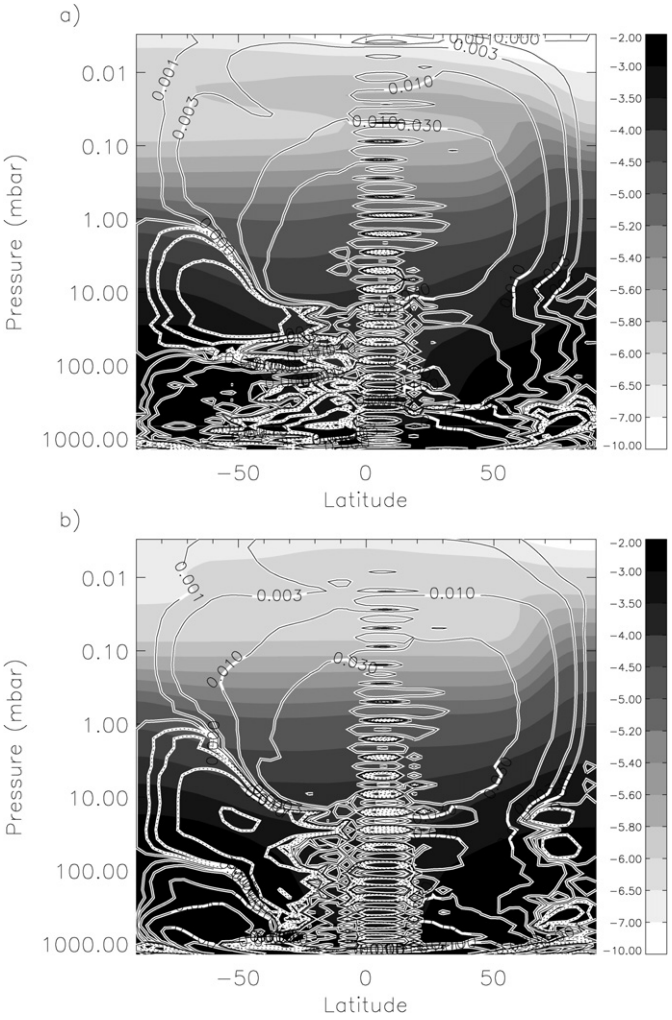

Fig. 8. Meridional maps (latitude–altitude) of a proxy for aerosol opacity distribution: (a) reference simulation, with haze source function at 0.01 mbar; (b) test simulation with haze source function elevated to 1 μbar. The proxy is defined as the sum of each fractal aerosol bin abundance (bins 5 to 10), multiplied by the number of monomers in the bin (1 to 10^5). The opacity from the spherical bins (bins 1 to 4) is neglected. The stream function is also shown with contours (units of 10^9 $kg\,s^{-1}$, solid line is clockwise rotation, dashed line is anti-clockwise).

must be taken with caution, as a simple test, because of the vertical limitation of the model. The change in the aerosol production height induces a rise of the detached haze layer, as shown in Fig. 8. This rise then has a significant influence on the thermal structure, which is presented in Fig. 9, to be compared with Fig. 1. The latitudinal temperature profile at 1.8 mbar for the test simulation is also shown in Fig. 2 for comparison. At this altitude, improving the haze distribution compared to Cassini observations yields significant improvement in the latitudinal temperature gradient in the summer hemisphere. Another consequence of the elevation of the haze production layer is to reduce the temperature at the top of the model, due to a slightly stronger net cooling in the uppermost layers (Fig. 9).

The modification of the thermal structure is coupled to modifications of the meridional circulation, and therefore affects the distribution of species (discussed in Section 5). The intensity of the meridional circulation is slightly weaker when the haze production source is elevated, as seen in Fig. 8 (essentially above 0.05 mbar). This weaker meridional circulation reduces the adiabatic heating in the winter polar mesosphere. Therefore, temperature in this region (above 0.01 mbar) is in better agreement with observations, but the thermal structure is still too warm at latitudes below 60° N.

Table 3
Available observations of the distribution of Titan's trace compounds at different seasons and latitudes

Observations	Reference	Season (*Ls*, degrees)	Latitude (degrees)	Altitude range (km)	Pressure range (mbar)
Voyager1/IRIS	Coustenis et al. (1991)	9	70° N	~175–275	~1.5 and 0.1
(latitudinal profiles)	Coustenis and Bézard (1995)	9	53° S–70° N		Contribution functions (see reference)
Ground-based	Tanguy et al. (1990)	130	Disk average	90–450	13–0.004 (HCN)
(vertical profiles)	Hidayat et al. (1997)	180	Disk average	100–345	9.5–0.035 (HCN)
	Marten et al. (2002)	180	Disk average	90–445	13–0.0045 (HCN)
				70–490	26–0.0017 (HC_3N)
				100–500	9.6–0.0012 (CH_3CN)
	Coustenis et al. (2003)	190	Disk average	80–250	20–0.3 (C_2H_2)
	Gurwell (2004)	300	Disk average	100–365	9.6–0.022 (HCN)
Cassini/CIRS	Vinatier et al. (2007)	300	15° S (Tb)	115–450	~6.5–0.004
(vertical profiles)	Vinatier et al. (2007)	300	80° N (T3)	155–490	~2–0.0018
				180–520	~1–0.0009 (HC_3N)
	Vinatier (2007)	300	54° S (T15)	110–500	8–0.001
	Teanby et al. (2007)	300	15° S (Tb)	120–350(450)	6–0.03(0.004) HCN(C_2H_2)
	Teanby et al. (2007)	300	15° S (Tb)	300–450	0.1–0.004 (HC_3N)
	Teanby et al. (2007)	300	82° N (T4)	150–310	1.5–0.04 (HCN, C_2H_2)
	Teanby et al. (2007)	300	82° N (T4)	200–310	0.4–0.04 (HC_3N)
(latitudinal profiles)	Coustenis et al. (2007b) Coustenis et al. (2007a)	300	(high S–high N)		Contribution functions (see references)
	Teanby et al. (2006, 2008)	300	80° S–80° N	140; 290	3 (HCN, C_2H_2); 0.1 (HC_3N)
(meridional maps)	Teanby et al. (2007)	300	80° S–80° N	140–500	3–0.002

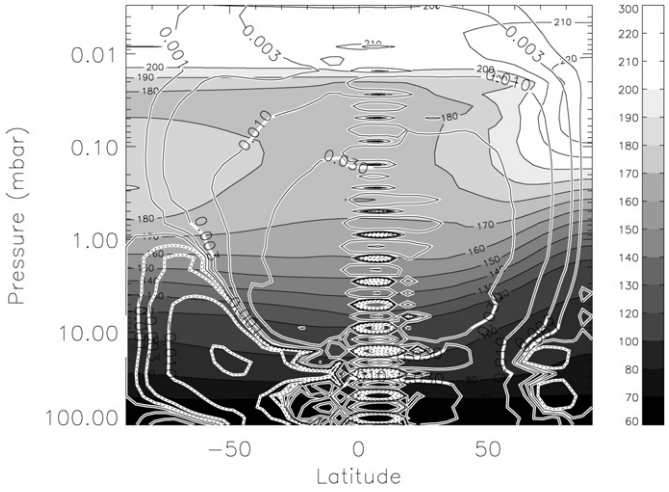

Fig. 9. Same figure as Fig. 1b, but for the test simulation with haze source function elevated to 1 μbar.

This discrepancy suggests that the dominant problem in this region may come from the shortcomings in the radiative cooling scheme, as discussed previously. At 80° N, the model is still too cold in the lower stratosphere (between the tropopause and 0.5 mbar), which may be related to the fact that the mean haze layer is not influenced by variations in the altitude of the haze production region, or to the latitudinal extension of the polar vortex, as it is discussed for the composition (see Section 5). The zonal wind is also slightly modified in this test simulation, especially in the mesosphere, due to a stronger impact of the opacity modifications on the mesospheric temperature field. The stratospheric jet is slightly more confined, both in latitude and altitude.

5. Distribution of trace compounds and implications for circulation

As discussed in Lebonnois et al. (2001) and Hourdin et al. (2004), dynamics also has an impact on atmospheric composition. Chemical species included in the 2D-CM and observed in Titan's atmosphere, act as tracers of atmospheric circulation because their photochemical lifetimes are often larger than typical dynamical timescales. These compounds are mostly well mixed in the stratospheric cell, between 10 and 0.01 mbar, except for the descending branch over the polar regions, which brings enriched air from the upper atmosphere (above ~400 km) where most of these compounds are mainly produced, into the lower stratosphere. Most species condense at the cold tropopause (~70 K), which constitutes a cold trap. Therefore, air rising from the tropopause in the summer ascending branch at the tropics contains significantly less abundances of chemical species than the ambient stratospheric air. The mechanisms that control the vertical concentration gradients are essentially chemistry and dynamics. The chemistry in the upper atmosphere controls the production of many species, and therefore their stratospheric abundances. The chemical fluxes at the top of the model (around 500 km) are thus very important for a good representation of the mean abundances in the stratosphere. For latitudinal gradients, vertical advection by dynamics (Brewer–Dobson cell) and condensation tend to strengthen contrasts, while latitudinal mixing by barotropic waves tends to reduce them. These latitudinal gradients are also affected by the vertical distance between the level at which they are observed and their condensation level: increased distance between observation and condensation levels means a larger effect of horizontal dissipation, and a reduced observed latitudinal contrasts.

5.1. Equatorial regions

Observations of Titan's stratospheric composition at different seasons and latitudes are summarized in Table 3. Plots of observed equatorial profiles compared to the 2D-CM simulation for many hydrocarbons and nitriles are shown in Fig. 10. The agreement between 2D-CM chemical distributions and observations is generally good, though it must be kept in mind that some upper boundary fluxes have been adjusted to improve the modeled abundances of some compounds (see Section 2). The available observational dataset covers more than one season: from disk-averaged ground-based observations during northern fall equinox (Hidayat et al., 1997) to Cassini mission observations in northern winter at 15° S (Teanby et al., 2006, 2007; Coustenis et al., 2007b; Vinatier et al., 2007). These observations are compared to the 2D-CM in Fig. 10. Only very small seasonal variations are seen at these low latitudes, both in the observations and in the model.

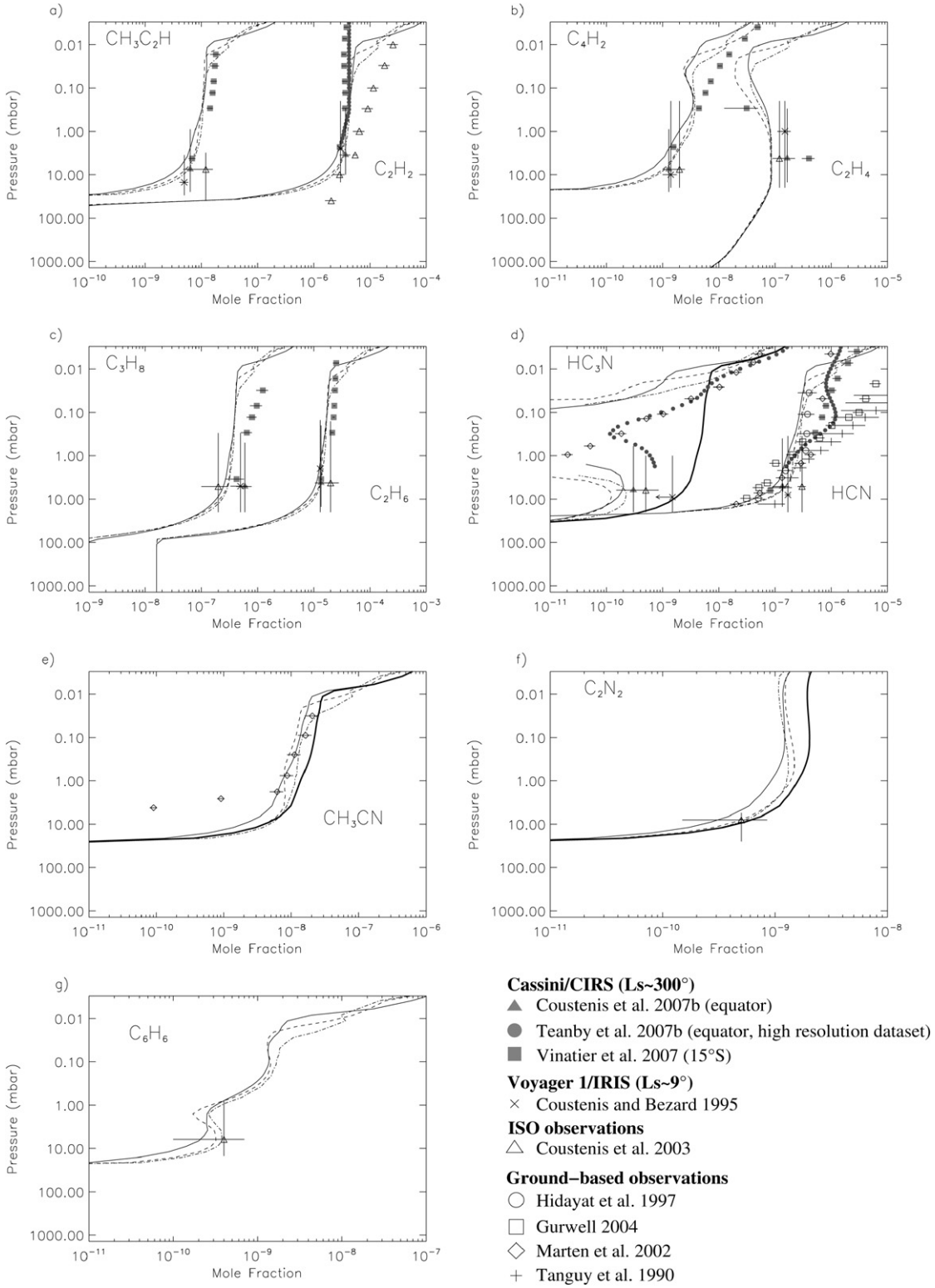

Fig. 10. Vertical profiles variations of chemical compounds in Titan's equatorial region: comparison between available observations (see legends for references) and the 2D-CM. The modeled profiles are taken for: 15° S, $Ls = 300°$ (solid line); equator, $Ls \sim 9°$ (dashed line); equator, $Ls \sim 180°$ (dash-dotted line). The heavy solid line shows HC_3N, C_2N_2 and CH_3CN in the case when no parameterization of polymerization is included. Available observations are (see Table 3): Cassini/CIRS, Voyager1/IRIS, ISO observations and ground-based observations.

The modeled hydrogen cyanide (HCN) vertical profile is in good agreement with disk-averaged ground-based observations by Hidayat et al. (1997) and Marten et al. (2002) during northern fall (Fig. 10d). ISO measurements in the same period (Coustenis et al., 2003) are slightly lower than other observations, and the 2D-CM. However, the vertical gradient of HCN derived from Cassini/CIRS observations at 15° S is stronger than for C_2H_2 or C_2H_6 (Fig. 10a and Fig. 10c, respectively). This is not the case in the 2D-CM results, where the vertical gradients of HCN, C_2H_2 and C_2H_6 are mutually very similar. The observed difference in vertical gradi-

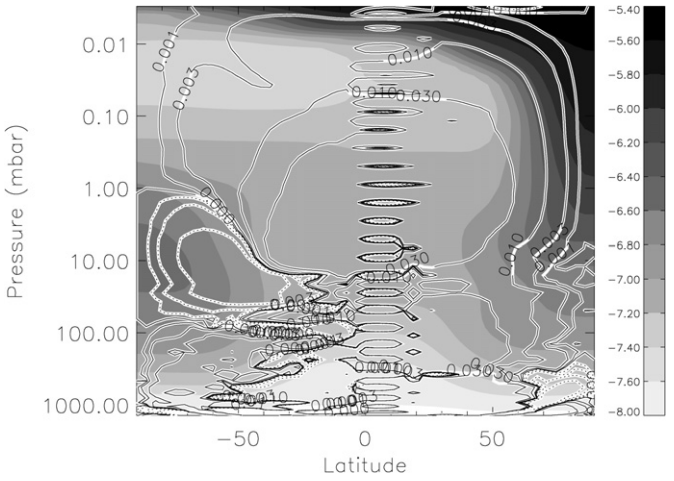

Fig. 11. Meridional map of C_2H_4 (latitude–altitude) from the 2D-CM during the Cassini epoch ($Ls \sim 300°$) (logscale). The stream function is also shown with contours (units of 10^9 kg s^{-1}, solid line is clockwise rotation, dashed line is anti-clockwise).

ent may be a diagnostic of chemical loss for HCN in the lower stratosphere with a timescale shorter than the meridional dynamical timescale, as proposed by Vinatier et al. (2007). Indeed, in simulations performed with the updated version of the Lebonnois et al. (2001) model, that were used to compute upper boundary fluxes (see Section 2), the parameterization of polymer formation does affect the HCN vertical profile, yielding a HCN concentration gradient different from that of C_2H_2 or C_2H_6, as observed. This model has the same photochemistry as the 2D-CM but uses a forced, analytical representation of the dynamics. The different behaviors between both models must be due to their different dynamics. In the 2D-CM, the dynamical mixing may be slightly too strong, masking the influence of the parameterized loss of HCN to polymer formation.

For ethylene (C_2H_4, Fig. 10b), at 15° S, we obtain a vertical mixing ratio profile that decreases with altitude in the stratosphere, which is in agreement with the Vinatier et al. (2007) observations, though the amplitude of the modeled effect is much less than observed. This negative vertical gradient in the lower stratosphere is interpreted as being due to photochemistry and dynamical transport, as illustrated in the meridional distribution of ethylene at the Cassini epoch, shown in Fig. 11. The enriched winter polar region induces enrichment in the equatorial lower stratosphere due to transport by the meridional circulation, at pressure levels around 5–10 mbar. The fact that this compound does not condense at Titan's tropopause may also play a role, allowing for larger abundances in the troposphere. This equatorial (vertical) enrichment in the lower stratosphere cannot be produced in 1-dimensional models, because of the sink due to photodissociation of C_2H_4 which peaks higher, near 0.1–0.01 mbar.

Though the modeled mean stratospheric abundance of diacetylene (C_4H_2, Fig. 10b) is in good agreement with observations at these low latitudes, it is sensitive to many model parameters such as: the abundances of other compound abundances; stratospheric photochemistry; and upper boundary flux (Hébrard et al., 2007). Therefore, it is difficult to derive any firm conclusions for this compound.

The case of HC_3N is unique: this compound is extremely sensitive to the parameterization of polymerization, as seen in Fig. 10d, which shows the difference in the profiles obtained with active parameterization (yielding a strong sink for HC_3N between 1 and 0.1 mbar), or without (homogeneous vertical profile). CH_3CN and C_2N_2 are also slightly sensitive to this process, as shown in Fig. 10e and Fig. 10f, respectively. This is not the case for other compounds. However, since this parameterization of polymerization processes may not be completely realistic, it is probable that the very steep profile observed for HC_3N compared to other compounds is diagnostic of a specific chemical sink in the lower stratosphere, as discussed above for the case of HCN.

5.2. Winter polar enrichment

Latitudinal distributions of trace compounds obtained in the 2D-CM during the Cassini ($Ls \sim 300°$) and Voyager ($Ls \sim 9°$) epochs are presented in Fig. 12, in comparison with profiles obtained from Cassini/CIRS (Coustenis et al., 2007a, 2007b) and Voyager1/IRIS (Coustenis and Bézard, 1995) observations. Such a comparison has also been performed in a recent analysis of Cassini/CIRS data by Teanby et al. (2008). As discussed in Coustenis et al. (2007b), the enrichment observed at high northern latitudes is slightly stronger after northern spring equinox than at northern mid-winter. Such an effect is visible in the 2D-CM, with a slightly deeper latitudinal gradient close to 50–60° N at the Voyager 1 epoch, compared to the Cassini epoch. This can be explained by the continuous increase of contrasts produced by the meridional circulation, until it reverses after northern spring equinox.

Teanby et al. (2007) have obtained meridional distributions for HCN and HC_3N from CIRS data, which are compared to the distributions obtained in the 2D-CM in Fig. 13. Enrichment at the high-northern latitudes, due to the descending circulation, is visible in the observations, though it seems to be confined closer to the pole, especially in the 0.1–0.01 mbar region. The HC_3N destruction due to the parameterization of the polymerization, seen in the modeled distribution, appears to be largely overestimated, but as previously discussed, the HC_3N abundance in the mid-stratosphere is extremely sensitive to this process.

Vertical profiles at 80° N (T3 flyby; Vinatier et al., 2007) and 82° N (T4 flyby; Teanby et al., 2007) have been retrieved from CIRS limb observations. At these high latitudes in the winter hemisphere, the modeled profiles of some compounds are, at a first glance, clearly different from the observations (Fig. 14).

For C_2H_2, C_2H_6 and C_3H_8 (Figs. 14a, 14c, and 14d, respectively), the observed vertical profiles are similar to those observed in the equatorial regions. These compounds have small vertical, latitudinal and temporal variations, and appear to be well mixed by the overall meridional circulation. The modeled enrichment in high northern latitudes is higher than observed. This is related to the strong vertical gradient between the uppermost levels of the 2D-CM where the upper boundary flux is implemented, and the levels below where large-scale mixing is efficient. This is model-dependent, and vertical extension of the model into the mesosphere is needed to test the impact of the mesospheric dynamics (which is still largely unknown) on the vertical profiles in this transition region.

For HCN (Fig. 14e), the enrichment observed in nadir data in the lower stratosphere is also seen in limb observations, and the 2D-CM yields a vertical profile approximately consistent with the observations, although there is a noticeable difference between the retrievals by Vinatier et al. (2007) (T3, 80° N) and Teanby et al. (2007) (T4, 82° N) due to differences in the projected sizes of the CIRS field-of-views between flybys.

The behavior of the C_2H_4, CH_3C_2H and C_4H_2 vertical profiles (Figs. 14b, 14a, and 14d, respectively) at 80° N is different: the enrichment observed in nadir data in the lower stratosphere is seen in limb observations, but only at pressures greater than 0.1 mbar. In the upper stratosphere, an abundance minimum is seen in the observed profiles at around 0.07 mbar, whereas the 2D-CM abundance profiles are well mixed all along the atmospheric column. Abundance minima are predicted by the model at lower latitudes, as shown for 50° N in Fig. 14, indicative of a region outside the

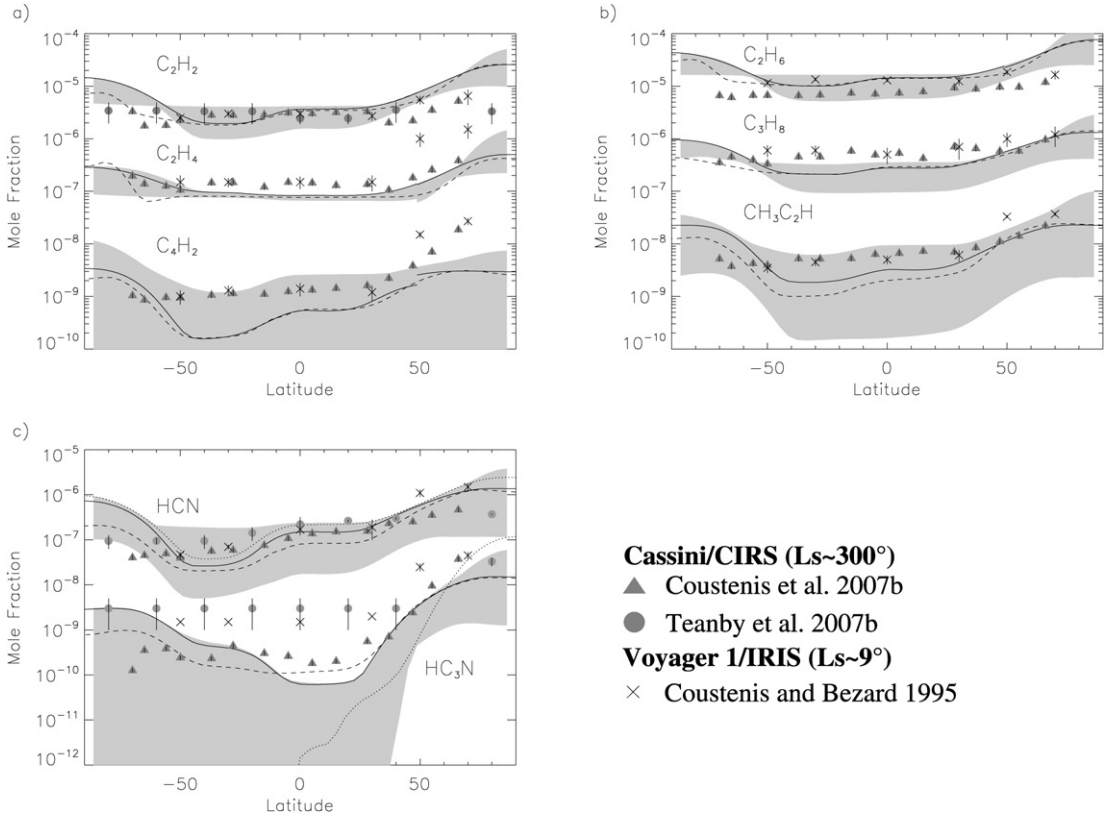

Fig. 12. Composition latitudinal profiles: comparison between modeled composition and observations at Voyager 1 and Cassini epochs (see legends for references). Observations: Cassini/CIRS during northern winter ($Ls \sim 300°$); Voyager1/IRIS during northern early spring ($Ls \sim 9°$). Simulation: Voyager 1 epoch (dashed line) profiles, at altitude corresponding to the maximum of the weighting functions for the corresponding observations (Coustenis and Bézard, 1995); Cassini epoch profiles, taken at the maximum of the weighting functions (dotted line for Teanby et al., 2007; solid line for Coustenis et al., 2007b in three different latitude regions, i.e. polar regions down to 50°, and in between). The light-gray region shows the range of modeled 2D-CM values within the half-width altitude range of the weighting functions (taken from Coustenis et al., 2007b).

main descent of air located within the polar vortex, as it is also visible in Figs. 11 and 13. Moreover, stratospheric minima have been clearly observed at 54° N for C_2H_2, C_4H_2 and HCN, and to a lesser extent, for C_2H_6 and HC_3N (Vinatier, 2007). Such profiles observed at 80° N may therefore be a diagnostic of the latitudinal extent of the polar vortex (as discussed above for Fig. 13), and of the intensity of the meridional circulation. As discussed in Section 4.3, the test simulation run with the haze production region moved up to the top level of the 2D-CM (1 μbar), shows variations in the meridional circulation, and therefore modifications in the distribution of chemical compounds. In the test simulation, the latitudinal extent of the polar region where the descending air is well mixed is modified when the meridional circulation is weakened. The high-stratospheric minima of chemical distributions are then obtained slightly closer to the pole than in the nominal simulation. The discrepancy between the modeled and observed thermal structure above the stratopause may also affect the strength and structure of the meridional circulation, thus affecting the latitudinal shape of the polar vortex. Also, the latitudinal resolution of the 2D-CM could affect the vortex latitudinal extension. Again, the 2-dimensional nature of this model is a potential source of discrepancy. Finally, another way to interpret the Cassini observations is that the polar vortex 3-dimensional structure may be highly distorted by waves, and that the T3 observations, though located at 80° N, have been sounding a region outside the heart of the polar vortex. Analysis of other flybys at high northern latitudes will be able to test this hypothesis. It may also be tested in a modeling context with a future 3-dimensional version of the circulation model.

It must also be noted that C_4H_2 and CH_3C_2H are very photochemically active in the upper stratosphere, which could affect our interpretation of dynamical transport discussed above. In the case of diacetylene (C_4H_2), this is illustrated by the peculiar behavior obtained in the simulations above 0.1 mbar, in the upper levels of the 2D-CM, where a strong minimum is seen very close to the pole (Fig. 14b). This minimum is related to the upper boundary flux reaching zero in this region during winter, associated with weak spatial mixing and strong photochemical destruction.

5.3. Summer pole

In extending the latitudinal coverage towards the southern summer polar regions, the CIRS observations (Flasar et al., 2005; Coustenis et al., 2007a, 2007b; Teanby et al., 2006, 2008) have revealed a strong disagreement with the modeled stratospheric distributions of minor compounds. In the summer hemisphere, the observed stratospheric abundances are globally uniform in latitude, whereas, in the model, the signature of a secondary meridional cell is obvious (Fig. 12). This cell is located in the 2D-CM meridional circulation between the ascending region around 30–40° S at the tropopause and the summer pole, and extends vertically in the lower stratosphere from roughly 60 to 1 mbar (see Fig. 1b). In this altitude region, the consequences of this cell on latitudinal profiles are a residual enrichment over the pole (from the previous winter season), and a decrease in abundance for condensing species around 30° S, in the ascending branch of the stratospheric cell, which brings tropospheric air into the stratosphere. This effect is stronger for compounds that are observed deeper in the stratosphere.

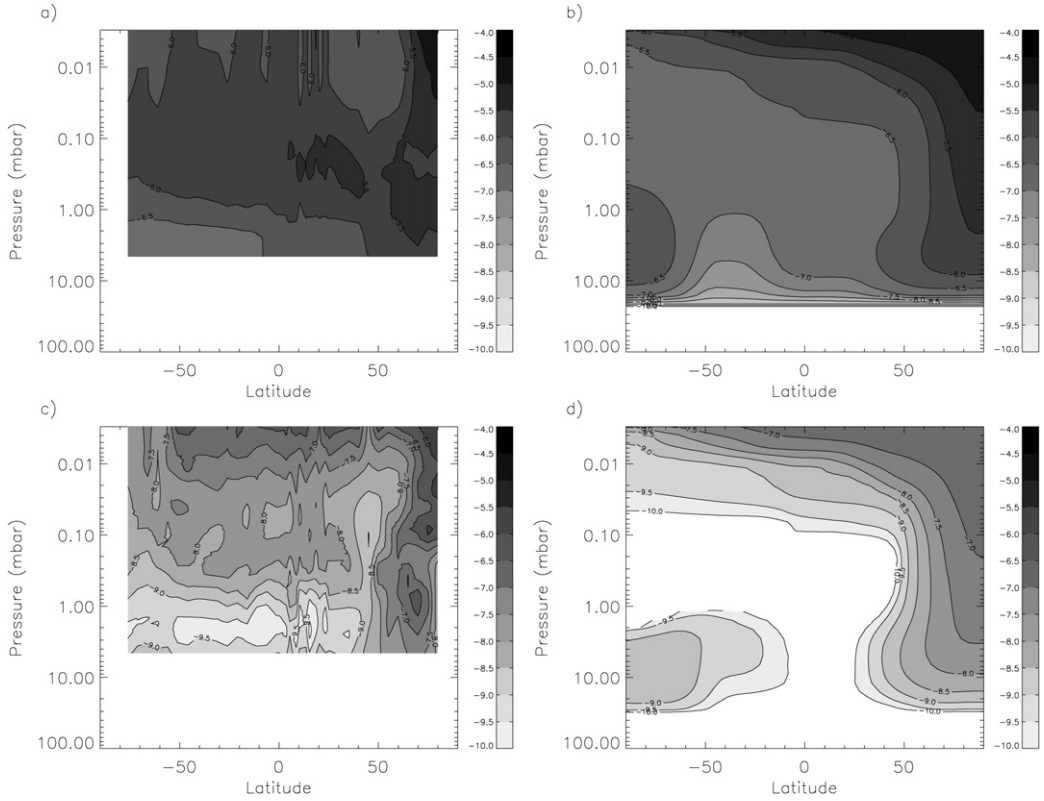

Fig. 13. Comparison between Teanby et al. (2007) retrievals (low-resolution dataset) and 2D-CM distributions for HCN (a: CIRS; b: 2D-CM) and HC_3N (c: CIRS; d: 2D-CM) meridional maps (latitude–altitude) during Cassini epoch ($Ls \sim 300°$) (logscale).

The existence of this secondary cell has some observational support: Roe et al. (2004) observed an accumulation of ethylene at the south pole (above 60° S) during late southern spring ($Ls \sim 240$), in agreement with the 2D-CM. In the current season, the reversal of the meridional circulation is complete, and the build-up of winter enrichment already well started. The secondary cell limits the erasing of the previous season enrichment by the ascending motions.

There are several hypotheses to reconcile the modeled distributions with the observations. Considering that the meridional circulation derived from the 2D-CM has successfully explained many of Titan's atmospheric features, there must be an ascending branch in the lower stratosphere. Since the CIRS observations do not see the corresponding depleted region, we propose three possible explanations: (1) this secondary cell is not present on the real Titan, and is a diagnostic of a structural problem of the 2D-CM; (2) due to weaker meridional circulation, this secondary cell is less extended vertically and less active, and the depleted region is located closer to the tropopause on Titan than in the model; (3) there is an additional horizontal mixing process that may be missing from the 2D-CM, which would limit the vertical extension of the depleted region. The extension of the model to 3 dimensions will help investigate hypothesis (1) and (3). This extension is currently under development. In the test simulation discussed previously, although the meridional circulation is slightly weakened, the impact on the southern latitudinal profiles is weak, with only a slightly smaller depletion at mid-latitudes.

The vertical profiles around 54° S deduced from CIRS observations during the T15 flyby (Vinatier, 2007) (not shown in this paper) may also be compared to the corresponding 2D-CM profiles. Both observed and modeled profiles in this region are very similar to equatorial observations. As seen in Fig. 13, latitudinal variations are much less significant in the summer hemisphere, compared to the winter hemisphere. Modeled vertical profiles are in good agreement with observations, because the effects due to the summer secondary meridional cell are visible only in the deepest region retrieved in observed vertical profiles (below roughly 1.3 mbar). For ethylene (C_2H_4), the vertical observed profile (Vinatier, 2007) is qualitatively reproduced, with a sink in the upper stratosphere (related to photodissociation). The gradient of hydrogen cyanide (HCN) is also well represented by the model.

6. Conclusion

The comparison between results of the 2-dimensional Titan circulation model developed at IPSL and available observations with a focus on recent Cassini/CIRS results, has been detailed in this work. The purpose of this paper is not to solve all the differences between the model and observations, but to draw a picture of the different processes present in the 2D-CM that can account for the main observed features. Given that observed chemical species are tracers of dynamics, a correct representation of chemical distributions, together with the aerosol and cloud descriptions, allows us first to validate the 2D-CM, and then to determine some diagnostics of Titan's stratospheric dynamics. The thermal structure, dynamics and composition are a coupled system. Modifications in thermal structure induce modifications of the meridional circulation, and therefore affects the chemical distributions.

The main results of this work are the following:

(1) Many characteristics of the observed thermal structure are reproduced in the 2D-CM, including increased temperatures in the upper stratosphere of the winter polar region due to adiabatic heating in the descending branch of the meridional circulation. The strong coupling between haze distribution, meridional circulation and thermal structure is shown to be realistically modeled. Some discrepancies between model and observations may be explained by the haze structure, its

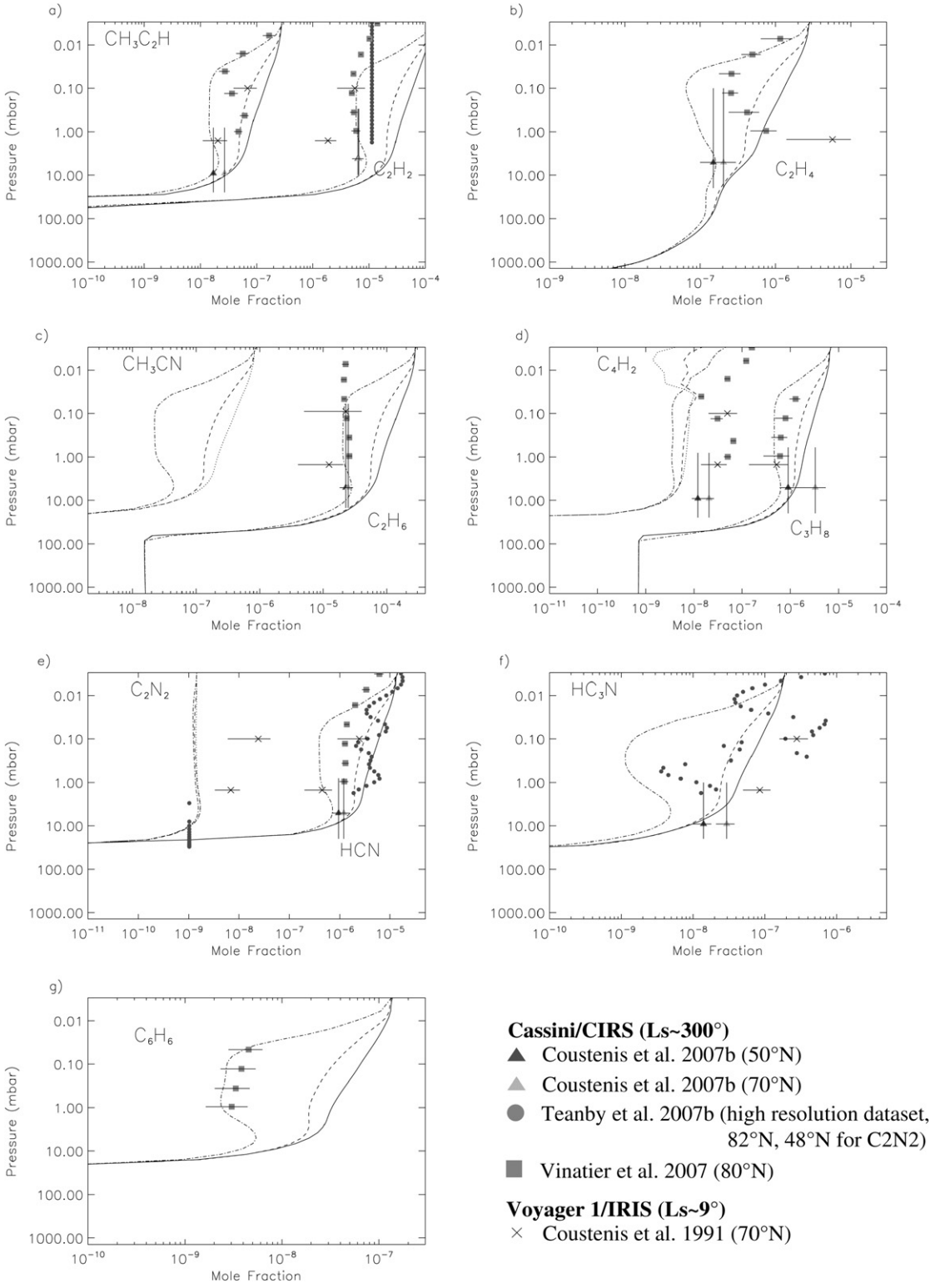

Fig. 14. Vertical variations of chemical compounds in the northern polar region: comparison between available observations (see legends for references) and the 2D-CM profiles. The modeled profiles are taken for: 50° N, $Ls \sim 300°$ (dash-dotted line); 70° N, $Ls \sim 300°$ (dashed line); 80° N, $Ls \sim 300°$ (solid line). Available observations are (see Table 3): Cassini/CIRS, (50° N, 70° N, 82° N, 48° N and 80° N); Voyager1/IRIS (70° N, $Ls = 9°$).

source being tuned to reproduce Voyager observations, and by the misrepresentation of mesospheric radiative effects, pointing to current limitations of the model at the upper boundary.

(2) Superrotation, with strong prograde zonal winds, is produced by the 2D-CM in good agreement with Cassini/CIRS, Huygens/DWE and stellar occultation observations (Hubbard et al., 1993; Sicardy et al., 2006). A Hadley-type meridional circulation, transporting angular momentum towards the winter pole, can account for the strong winter zonal jet produced in high latitudes. This jet becomes barotropically unstable on its equatorward flank, producing waves (parameter-

ized in the 2-dimensional model), which redistribute angular momentum towards the equator (Gierasch–Rossow mechanism).

(3) (a) Overall, chemical distributions are well reproduced in equatorial regions, though it must be kept in mind that some upper boundary fluxes have been adjusted to improve the modeled abundances of some compounds. The enrichment of ethylene in the lower stratosphere at 15° S is explained by dynamical transport from the winter polar region.

(b) Near the winter pole (80° N), the observed enrichment at high northern latitudes, slightly stronger after spring equinox than for mid-winter, is captured by the 2D-CM. However, there is still a strong disagreement between observed and modeled profiles: some compounds (C_4H_2, CH_3C_2H) have an abundance minimum near 0.05 mbar in the observed vertical profiles, whereas 2D-CM profiles are well mixed all along the atmospheric column. The modeled profiles exhibit a small minimum in chemical distributions for lower latitudes, in regions outside the influence of the polar vortex. When the altitude of the haze production is increased, latitudinal extension of the polar vortex is reduced and high-stratospheric minima in the vertical profiles of mixing ratios are obtained slightly closer to the pole. It might also be possible that large scale waves are present on the polar vortex sides, producing important longitudinal features. However, the observed profiles are difficult to reconcile with dynamical features.

(c) In the summer hemisphere, the model produces a secondary cell in the lower stratosphere, which maintains an enrichment over the summer pole and a depleted region around 30° S. This cell is coupled to the polar enrichment of the haze—still present during summer. The signature of this cell is not present in Cassini/CIRS data, whereas some previous observations support the existence of an accumulation of ethylene over the south pole during late southern spring (Roe et al., 2004). It is possible that some horizontal mixing processes are missing due to the 2-dimensional nature of the model. Outside the secondary cell region, vertical profiles are in good agreement with Cassini/CIRS observations at 54° S.

The IPSL 2-dimensional circulation model of Titan's atmosphere reproduces the main observed features of the global atmospheric behavior, at two different seasons: the Voyager 1 season, northern spring equinox, as well as the Cassini season, northern mid-winter. This is a significant confirmation that the dominant processes present in this complex atmosphere are correctly modeled, including many couplings between winds, thermal structure, haze and composition. However, the remaining discrepancies point to limitations of the model (2 dimensions, restricted vertical extension), and to possible missing processes (planetary waves not parameterized, gravitational tides, role of topography, and so on). The restricted 2-dimensional nature of the model is in particular a potential source of uncertainties, and investigations need to be done using a future 3-dimensional version of the circulation model.

References

Achterberg, R.K., Conrath, B.J., Gierasch, P.J., Flasar, F.M., Nixon, C.A., 2008. Titan's middle-atmospheric temperatures and dynamics observed by the Cassini Composite Infrared Spectrometer. Icarus 194, 263–277.

Bézard, B., Coustenis, A., McKay, C.P., 1995. Titan's stratospheric temperature asymmetry: A radiative origin? Icarus 113, 267–276.

Bird, M.K., and 14 colleagues, 2005. The vertical profile of winds on Titan. Nature 438, 1–3.

Borysow, A., Tang, C., 1993. Far infrared CIA spectra of N_2–CH_4 pairs for modeling of Titan's atmosphere. Icarus 105, 175–183.

Cabane, M., Chassefière, E., Israel, G., 1992. Formation and growth of photochemical aerosols in Titan's atmosphere. Icarus 96, 176–189.

Coll, P., Coscia, D., Smith, S., Gazeau, M.-C., Ramirez, S.I., Cernogora, G., Israël, G., Raulin, F., 1999. Experimental laboratory simulation of Titan's atmosphere: Aerosols and gas phase. Planet. Space Sci. 47, 1331–1340.

Courtin, R., 1988. Pressure-induced absorption coefficients for radiative transfer calculations in Titan's atmosphere. Icarus 75, 245–254.

Coustenis, A., Bézard, B., 1995. Titan's atmosphere from Voyager infrared observations. IV. Latitudinal variations of temperature and composition. Icarus 115, 126–140.

Coustenis, A., Bézard, B., Gautier, D., Marten, A., Samuelson, R., 1991. Titan's atmosphere from Voyager infrared observations. III. Vertical distributions of hydrocarbons and nitriles near Titan's north pole. Icarus 89, 152–167.

Coustenis, A., Salama, A., Schulz, B., Ott, S., Lellouch, E., Encrenaz, T., Gautier, D., Feuchtgruber, H., 2003. Titan's atmosphere from ISO mid-infrared spectroscopy. Icarus 161, 383–403.

Coustenis, A., Jennings, D.E., Nixon, C.A., Achterberg, R.K., Conrath, B.J., Bjoraker, G., Vinatier, S., Teanby, N., Romani, P., Carlson, R., Royer, E., Flasar, F.M., 2007a. Titan's trace gaseous composition: Three years into the Cassini–Huygens mission. Bull. Am. Astron. Soc. 39. 47.06.

Coustenis, A., and 24 colleagues, 2007b. The composition of Titan's stratosphere from Cassini/CIRS mid-infrared spectra. Icarus 189, 35–62.

Flasar, F.M., Conrath, B.J., 1990. Titan's stratospheric temperatures: A case for dynamical inertia? Icarus 85, 346–354.

Flasar, F.M., Samuelson, R.E., Conrath, B.J., 1981. Titan's atmosphere: Temperature and dynamics. Nature 292, 693–698.

Flasar, F.M., and 44 colleagues, 2005. Titan's atmospheric temperatures, winds, and composition. Science 308, 975–978.

Forget, F., Hourdin, F., Fournier, R., Hourdin, C., Talagrand, O., Collins, M., Lewis, S.R., Read, P.L., Huot, J.-P., 1999. Improved general circulation models of the martian atmosphere from the surface to above 80 km. J. Geophys. Res. 104 (E10), 24155–24176.

Fulchignoni, M., and 42 colleagues, 2005. In situ measurements of the physical characteristics of Titan's environment. Nature 438, 1–7.

Gierasch, P., 1975. Meridional circulation and the maintenance of the Venus atmospheric rotation. J. Atmos. Sci. 32, 1038–1044.

Gurwell, M.A., 2004. Submillimeter observations of Titan: Global measures of stratospheric temperature CO, HCN, HC_3N, and the isotopic ratios. Astrophys. J. 616, L7–L10.

Hébrard, E., Dobrijevic, M., Bénilan, Y., Raulin, F., 2006. Photochemical kinetics uncertainties in modeling Titan's atmosphere: A review. J. Photochem. Photobiol. C 7 (4), 211–230.

Hébrard, E., Dobrijevic, M., Bénilan, Y., Raulin, F., 2007. Photochemical kinetics uncertainties in modeling Titan's atmosphere: First consequences. J. Photochem. Astrobiol. 7, 211–230.

Hidayat, T., Marten, A., Bézard, B., Gautier, D., Owen, T., Matthews, H.E., Paubert, G., 1997. Millimeter and submillimeter heterodyne observations of Titan: Retrieval of the vertical profile of HCN and the $^{12}C/^{13}C$ ratio. Icarus 126, 170–182.

Hourdin, F., Armengaud, A., 1999. Test of a hierarchy of finite-volume schemes for transport of trace species in an atmospheric general circulation model. Mon. Weather Rev. 127, 822–837.

Hourdin, F., Talagrand, O., Sadourny, R., Courtin, R., Gautier, D., McKay, C.P., 1995. Numerical simulation of the general circulation of the atmosphere of Titan. Icarus 117, 358–374.

Hourdin, F., Lebonnois, S., Luz, D., Rannou, P., 2004. Titan's stratospheric composition driven by condensation and dynamics. J. Geophys. Res. 109. E12005, 15 pp.

Hourdin, F., and 13 colleagues, 2006. The LMDZ4 general circulation model: Climate performance and sensitivity to parameterized physics with emphasis on tropical convection. Clim. Dynam. 27, 787–813.

Hubbard, W.B., and 45 colleagues, 1993. The occultation of 28 Sgr by Titan. Astron. Astrophys. 269, 541–563.

Lebonnois, S., 2005. Benzene and aerosol production in Titan and Jupiter's atmospheres: A sensitivity study. Planet. Space Sci. 53 (5), 486–497.

Lebonnois, S., Toublanc, D., Hourdin, F., Rannou, P., 2001. Seasonal variations in Titan's atmospheric composition. Icarus 152, 384–406.

Lebonnois, S., Bakes, E., McKay, C.P., 2002. Transition from gaseous compounds to aerosols in Titan's atmosphere. Icarus 159, 505–517.

Lebonnois, S., Bakes, E., McKay, C.P., 2003a. Atomic and molecular hydrogen budget in Titan's atmosphere. Icarus 161, 474–485.

Lebonnois, S., Hourdin, F., Rannou, P., Luz, D., Toublanc, D., 2003b. Impact of the seasonal variations of ethane and acetylene distributions on the temperature field of Titan's stratosphere. Icarus 163, 164–174.

Lindal, G.F., Wood, G.E., Hotz, H.B., Sweetnam, D.N., Eshleman, V.R., Tyler, G.L., 1983. The atmosphere of Titan: An analysis of the Voyager 1 radio occultation measurements. Icarus 53, 348–363.

Luz, D., Hourdin, F., 2003. Latitudinal transport by barotropic waves in Titan's stratosphere. I. General properties from a horizontal shallow–water model. Icarus 166, 328–342.

Luz, D., Hourdin, F., Rannou, P., Lebonnois, S., 2003. Latitudinal transport by barotropic waves in Titan's stratosphere. II. Results from a coupled dynamics–microphysics–photochemistry GCM. Icarus 166, 343–358.

Marouf, E., and 15 colleagues, 2006. Evidence for likely liquid hydrocarbons on Titan's surface from Cassini Radio Science bistatic scattering observations. In: AGU Meeting.

Marten, A., Hidayat, T., Biraud, Y., Moreno, R., 2002. New millimeter heterodyne observations of Titan: Vertical distributions of nitriles HCN, HC_3N, CH_3CN, and the isotopic ratio $^{15}N/^{14}N$ in its atmosphere. Icarus 158, 532–544.

Mitchell, J.L., Pierrehumbert, R.T., Frierson, M.W., Caballero, R., 2006. The dynamics behind Titan's methane cloud. Proc. Natl. Acad. Sci. 103 (49), 18421–18426.

Niemann, H.B., and 17 colleagues, 2005. The abundances of constituents of Titan's atmosphere from the GCMS instrument on the Huygens probe. Nature 438, 1–6.

Porco, C.C., and 35 colleagues, 2005. Imaging of Titan form the CASSINI spacecraft. Nature 434, 159–168.

Rannou, P., Cabane, M., Chassefière, E., Botet, R., McKay, C.P., Courtin, R., 1995. Titan's geometric albedo: Role of the fractal structure of the aerosols. Icarus 118, 355–372.

Rannou, P., Cabane, M., Botet, R., Chassefière, E., 1997. A new interpretation of scattered light measurements at Titan's limb. J. Geophys. Res. 102 (E5), 10997–11013.

Rannou, P., Hourdin, F., McKay, C.P., 2002. A wind origin for Titan's haze structure. Nature 418, 853–856.

Rannou, P., Hourdin, F., McKay, C.P., Luz, D., 2004. A coupled dynamics–microphysics model of Titan's atmosphere. Icarus 170, 443–462.

Rannou, P., Lebonnois, S., Hourdin, F., Luz, D., 2005. Titan atmosphere database. Adv. Space Res. 36, 2194–2198.

Rannou, P., Montmessin, F., Hourdin, F., Lebonnois, S., 2006. The latitudinal distribution of clouds on Titan. Science 311, 201–205.

Roe, H.G., de Pater, I., McKay, C.P., 2004. Seasonal variation of Titan's stratospheric ethylene (C2H4) observed. Icarus 169, 440–461.

Samuelson, R., Nath, N., Borysow, A., 1997. Gaseous abundances and methane supersaturation in Titan's troposphere. Planet. Space Sci. 45, 959–980.

Sekine, Y., Lebonnois, S., Imanaka, H., Matsui, T., Bakes, E., McKay, C.P., Khare, B.N., Sugita, S., 2008. The role of organic haze in Titan's atmospheric chemistry. II. Effect of heterogeneous reaction to the hydrogen budget and chemical composition of the atmosphere. Icarus 194, 201–211.

Shemansky, D.E., Stewart, A.I.F., West, R.A., Esposito, L.W., Hallett, J.T., Liu, X., 2005. The Cassini UVIS stellar probe of the Titan atmosphere. Science 308, 978–982.

Sicardy, B., and 51 colleagues, 2006. The two Titan stellar occultations of 14 November 2003. J. Geophys. Res. 111.

Sotin, C., and 25 colleagues, 2005. Release of volatiles from a possible cryovolcano from near-infrared imaging of Titan. Nature 435, 786.

Stofan, E.R., and 35 colleagues, 2006. Mapping of Titan: Results from the first Titan radar passes. Icarus 185, 443–456.

Tanguy, L., Bézard, B., Marten, A., Gautier, D., Gérard, E., Paubert, G., Lecacheux, A., 1990. Stratospheric profile of HCN on Titan from millimeter observations. Icarus 85, 43–57.

Teanby, N.A., Irwin, P.G.J., de Kok, R., Nixon, C.A., Coustenis, A., Bézard, B., Calcutt, S.B., Bowles, N.E., Flasar, F.M., Fletcher, L., Howett, C., Taylor, F.W., 2006. Latitudinal variations of HCN, HC_3N and C_2N_2 in Titan's stratosphere derived from Cassini CIRS data. Icarus 181, 243–255.

Teanby, N.A., Irwin, P.G.J., de Kok, R., Vinatier, S., Bézard, B., Nixon, C.A., Flasar, F.M., Calcutt, S.B., Bowles, N.E., Fletcher, L., Howett, C., Taylor, F.W., 2007. Vertical profiles of HCN, HC_3N and C_2H_2 in Titan's atmosphere derived from Cassini/CIRS data. Icarus 186, 364–384.

Teanby, N.A., Irwin, P.G.J., de Kok, R., Nixon, C.A., Coustenis, A., Royer, E., Calcutt, S.B., Bowles, N.E., Fletcher, L., Howett, C., Taylor, F.W., 2008. Global and temporal variations in hydrocarbons and nitriles in Titan's stratosphere for northern winter observed by Cassini/CIRS. Icarus 193, 595–611.

Tobie, G., Lunine, J.I., Sotin, C., 2006. Episodic outgassing as the origin of atmospheric methane on Titan. Nature 440, 61–64.

Tokano, T., Neubauer, F.M., Laube, M., McKay, C.P., 2001. Three-dimensional modeling of the tropospheric methane cycle on Titan. Icarus 153, 130–147.

Tokano, T., McKay, C.P., Neubauer, F.M., Atreya, S.K., Ferri, F., Fulchignoni, M., Niemann, H.B., 2006. Methane drizzle on Titan. Nature 442, 432–435.

Tomasko, M.G., and 39 colleagues, 2005. Rain, winds and haze during the Huygens probe's descent to Titan's surface. Nature 438, 1–14.

Toublanc, D., Parisot, J.P., Brillet, J., Gautier, D., Raulin, F., McKay, C.P., 1995. Photochemical modeling of Titan's atmosphere. Icarus 113, 2–26.

Vervack Jr., R.J., Sandel, B.R., Strobel, D.F., 2004. New perspectives on Titan's upper atmosphere from a reanalysis of Voyager 1 UVS solar occultations. Icarus 170, 91–112.

Vinatier, S., 2007. Analyse des spectres infrarouge thermiques de l'atmosphère de Titan enregistrés par l'instrument CIRS à bord de Cassini. Ph.D. thesis, Université Paris VII.

Vinatier, S., Bézard, B., Fouchet, T., Teanby, N.A., de Kok, R., Irwin, P., Conrath, B.J., Nixon, C.A., Romani, P.N., Flasar, F.M., Coustenis, A., 2007. Vertical abundance profiles of hydrocarbons in Titan's atmosphere at 15° S and 80° N retrieved from Cassini/CIRS spectra. Icarus 188, 120–138.

Vuitton, V., Doussin, J.-F., Bénilan, Y., Raulin, F., Gazeau, M.-C., 2006. Experimental and theoretical study of hydrocarbon photochemistry applied to Titan stratosphere. Icarus 185, 287–300.

Waite Jr., J.H., and 21 colleagues, 2005. Ion Neutral Mass Spectrometer results from the first flyby of Titan. Science 308, 982–986.

Wilson, E.H., Atreya, S.K., 2003. Chemical sources of haze formation in Titan's atmosphere. Planet. Space Sci. 51 (14–15), 1017–1033.

Wilson, E.H., Atreya, S.K., 2004. Current state of modeling the photochemistry of Titan's mutually dependent atmosphere and ionosphere. J. Geophys. Res. 109. E06002, 39 pp.